



HAL
open science

Meta-analysis of radiocesium contamination data in Japanese cedar and cypress forests over the period 2011–2017

Marc Andre Gonze, Philippe Calmon, Pierre Hurtevent, Frederic Coppin

► To cite this version:

Marc Andre Gonze, Philippe Calmon, Pierre Hurtevent, Frederic Coppin. Meta-analysis of radiocesium contamination data in Japanese cedar and cypress forests over the period 2011–2017. *Science of The Total Environment*, 2021, 750 (142311), pp.1-20. 10.1016/j.scitotenv.2020.142311 . hal-02982031

HAL Id: hal-02982031

<https://hal.science/hal-02982031>

Submitted on 28 Oct 2020

HAL is a multi-disciplinary open access archive for the deposit and dissemination of scientific research documents, whether they are published or not. The documents may come from teaching and research institutions in France or abroad, or from public or private research centers.

L'archive ouverte pluridisciplinaire **HAL**, est destinée au dépôt et à la diffusion de documents scientifiques de niveau recherche, publiés ou non, émanant des établissements d'enseignement et de recherche français ou étrangers, des laboratoires publics ou privés.



Distributed under a Creative Commons Attribution - NonCommercial - NoDerivatives 4.0 International License

Manuscript Number:

Title: Meta-analysis of radiocesium contamination data in Japanese cedar and cypress forests over the period 2011-2017

Article Type: Review Article

Keywords: Cesium
Fukushima forests
data review
dynamic model

Corresponding Author: Mr. marc-andre gonze,

Corresponding Author's Institution: IRSN

First Author: marc-andre gonze

Order of Authors: marc-andre gonze; philippe calmon; pierre hurtevent;
frederic coppin

Abstract: Since Fukushima accident, dozens of field studies have been conducted in order to quantify and understand the behaviour of radiocesium (^{137}Cs) fallouts in contaminated forests of Fukushima and neighbouring prefectures. In this paper, we carry out a detailed review of data acquired over 2011-2017 in Japanese cedar and cypress plantations, focusing on aerial tree organs, soil layers and tree-to-soil depuration fluxes. To enable comparison and reinforce the consistency between sites, radiological measurements were normalized by the deposit and interpolated onto the same spatio-temporal frame. Despite some (poorly explained) residual variability, we derived a "mean" pattern by log-averaging data among sites. These results were analyzed with the help of a simple dynamic model and discussed in the light of post-Fukushima literature. We demonstrated that the activity levels and dynamics in the forest compartments were consistent and generally well reproduced by the mass balance model, for values of the interception fraction between 0.7-0.85. The analysis indicated that about 5% of the initial deposit remained in the aerial vegetation after 6 years, more than two thirds of intercepted ^{137}Cs being transferred to the soil due to throughfall. The simulations indicated that foliar uptake might have contributed between 40% and 100% to the activity transferred to stem wood. The activity concentration in canopy organs rapidly decreased in the first few months then more slowly, according to an effective half-life of about 1.6 years. The activity level in the organic layer peaked in summer 2011 then decreased according to an effective half-life of 2.2 years. After a rapid increase in 2011, the contamination of mineral horizons continued to increase more slowly, 85% of ^{137}Cs incoming from the organic layer being retained in the 0-5 cm layer, according to a mean residence time much longer than in the upper layer (7.5 against 1.5 years).

Suggested Reviewers: shoji hashimoto
FFPRI
shojih@ffpri.affrc.go.jp

laure gandois
ENSAT
laure.gandois@ensat.fr

kazuya nishina
NIES
nishina.kazuya@nies.go.jp

jordi vives i battle
SCK-CEN
Jordi.vives.i.batlle@sckcen.be

danyl perez sanchez
CIEMAT
d.perez@ciemat.es

Opposed Reviewers:

Dear Dr. M. GUSTIN

It is with pleasure that we submit the attached manuscript, "*Meta-analysis of radiocesium contamination data in Japanese cedar and cypress forests over the period 2011-2017*" for your consideration as a **Review article** within Science of the Total Environment.

Forests are particularly sensitive ecosystems due to the efficiency of canopies to intercept atmospheric pollution and the long-lasting immobilization and recycling of deposited pollutants. Due to its long physical half-life (i.e. 30 years), ¹³⁷Cs contamination induced by the Fukushima accident will dominate in the next decades. A long-term and scientifically-based management of contaminated forest environments is thus of great environmental, economic and social concerns for Japanese authorities.

In this paper, we carry out a detailed review and analysis of ~50 field studies conducted over the period 2011 – 2017 in ~40 Japanese cedar and cypress plantations of Fukushima and neighbouring prefectures. This work is a logical continuation of our previous meta-analysis (*Gonze and Calmon, 2017 - Meta-analysis of radiocesium contamination data in Japanese forest trees over the period 2011-2013. STOTEN 601-602*) which is here extended to the period 2014-2017 and the forest soil. Further, the database integrates new site-specific observations, notably short-term measurements of depuration fluxes, and some modifications in preexisting data after revision by their authors. Finally, the methodologies for processing data as well as the dynamic model for quantifying transfer processes have been improved.

The analysis highlights the overall coherence between site-specific observations, despite the variety of experimental protocols and differences in ecological, soil or climatic characteristics of the forest stands. Assuming that all sites conformed to the same pattern (within a residual variability), we derive a "mean" representative evolution of radiocesium over the 6-yr period by log-averaging data among sites and quantifying the residual dispersion. This "mean" evolution is analysed with the help of the above-mentioned process-based model and discussed in the light of an abundant post-Fukushima literature (about ~150 publications). We demonstrate that the activity levels and dynamics observed in all compartments of the forest are consistent and generally well reproduced by the model. We also provide numerical estimates of the key transfer parameters and attempt to quantify the respective contributions of each transfer process involved in the recycling of radiocesium. Beyond the results, we are convinced that the dataset constituted in this study will undoubtedly help improving forest models developed after the Chernobyl accident or currently being tested against Fukushima observations. It worth noting that our dataset recently served as a reference scenario in an international workshop (Japan, France and UK) on models inter-comparison (to be published soon).

Many readers of STOTEN will find the article of interest because it focuses on a topic that continues to raise scientific questions and has implications for ecological and human health (i.e. nuclear energy in general, and specifically the nuclear accident at Fukushima). More globally, many of your readers are interested in the atmospheric deposition of contaminants, their recycling within forest ecosystems and the uncertainties associated with field measurements and environmental modelling. Although our work focused on a radioactive contaminant, the knowledge developed in this study is also pertinent to many non-radioactive pollutants.

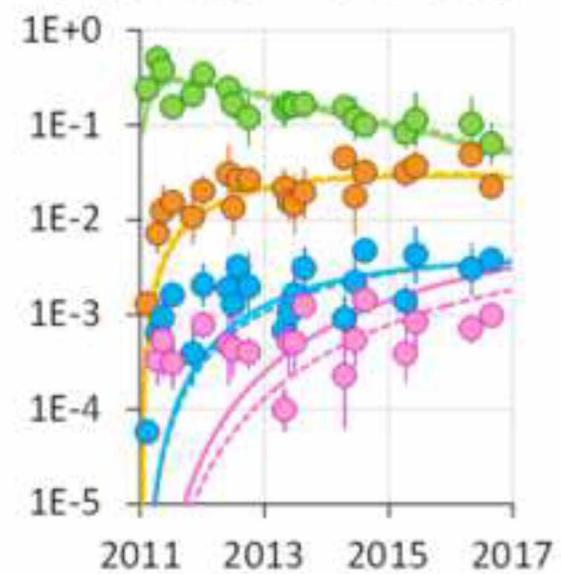
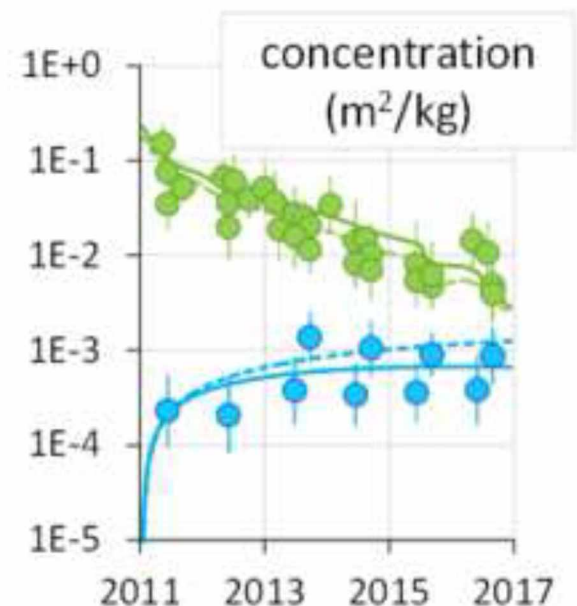
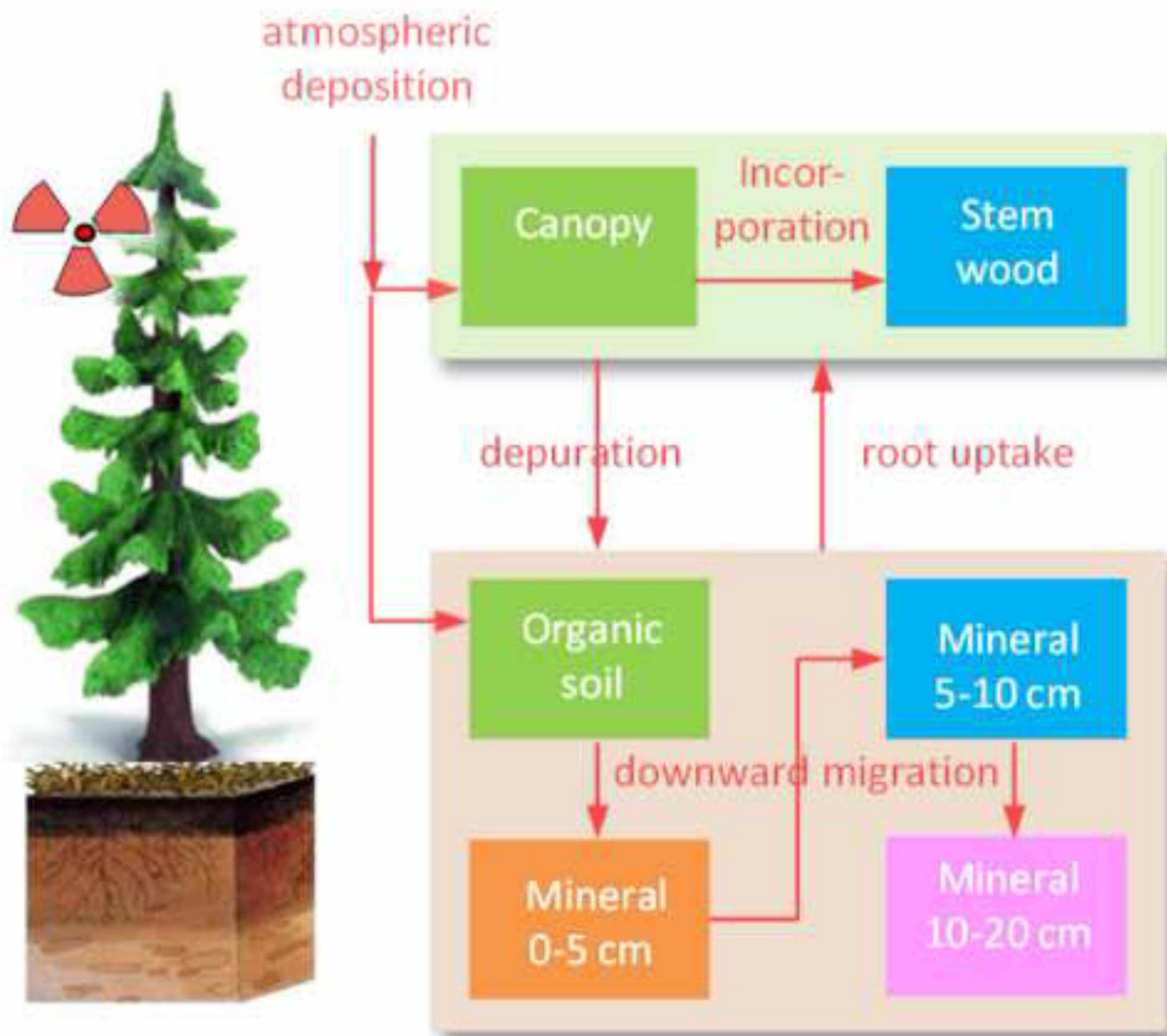
The manuscript has not been previously published, in whole or in part, and it is not under consideration by any other journal. Additionally, we have followed the guidelines required by your journal and provided a list of possible reviewers. All authors are aware of and accept responsibility for the manuscript.

Thanking you for your consideration of the article, Dr. M. GUSTIN, we look forward to receiving the reviews.

Sincerely,

Dr. Marc-André GONZE

Institute for Radiological Protection and Nuclear Safety (IRSN), Environmental Research Division, BP 3 - 13115 St-Paul-lez-Durance Cedex, France



1 **HIGHLIGHTS**

2

3 • Field studies on ^{137}Cs contamination in Japanese coniferous forests were reviewed

4 • A detailed spatio-temporal database was established for the period 2011-17

5 • The analysis highlights the consistency of data despite some residual variability

6 • Generic evolutions of ^{137}Cs in tree organs and soil layers were derived

7 • These results were analyzed and discussed thanks to a simple dynamic model

1 Introduction

2 In March 2011, the Fukushima Dai-ichi Nuclear Power Plant (FDNPP) accident led to massive
3 atmospheric deposits of radionuclides on the terrestrial environments, such as radiocesium and
4 radioiodine. Due to its long physical half-life (30.04 years), ^{137}Cs has become over the years the major
5 contributor to the long-lasting contamination in the impacted territories of Fukushima and neighboring
6 prefectures. Forests which occupy up to 75% of the most severely affected areas (MAFF, 2011;
7 Hashimoto et al., 2012; Yoshihara et al., 2013; Kato and Onda, 2018) are of concern because of their
8 valuable ecosystem services (e.g. timber, food production, recreational services) and their long-term
9 radiological impact on humans and biota through direct or indirect pathways (e.g. external exposure,
10 food-chain, releases through watershed erosion or forest fires). Among them, coniferous plantations of
11 Japanese cedars (*Cryptomeria japonica*) and cypresses (*Chamaecyparis obtusa*) are of particular
12 interest because of timber production (e.g. Japanese Forestry Agency, 2019) as well as of the richness
13 of field monitoring data that have since been acquired at many sites.

14 Since the accident, dozens of field studies have been conducted in Fukushima coniferous forests
15 to gain a clearer understanding of the various biological, physical and chemical processes involved in
16 the dissemination of radiocesium within the soil-tree system and quantify their respective contribution
17 on the short (months) and mid term (years) after deposition. Despite the disparity of the investigated
18 sites, time observation windows and experimental strategies deployed, there were a lot of common
19 features in the observations, to such a point that it is not unreasonable to draw a generic outline of
20 radiocesium dynamics in these forests over the first six years, at least qualitatively.

21 At time of atmospheric deposition, airborne radiocesium (^{137}Cs) was efficiently captured by
22 evergreen coniferous canopies through the interception of either particulate radiocesium or
23 contaminated water droplets (where/when fog or precipitation occurred). Several comparative studies
24 demonstrated that interception mechanisms were more efficient than in deciduous broadleaf forests, or
25 even mixed forests, due to the persistence of their foliage in winter season (e.g. MAFF, 2011, 2012;
26 Koarashi et al. 2012b; Kato et al., 2017). The proportion of the deposit intercepted by the aerial

27 biomass could not be measured, except at very few sites (Kato et al., 2012a; Nishikiori et al., 2019),
28 because most of the comprehensive field studies started not sooner than in summer 2011. Based on a
29 meta-analysis of field studies conducted between 2011 and 2013, Gonze and Calmon (2017) attempted
30 to infer, based on mass budget considerations, an average interception value for their selected sites,
31 which was estimated to about 90% for coniferous forests under the assumption that root uptake of
32 radiocesium by tree vegetation was negligible over this period. After deposition, coniferous vegetation
33 quite rapidly depurated over the first few months due mainly to the leaching by rainfall of freshly
34 contaminated canopy surfaces (i.e. throughfall) and, on the longer term, the contribution of litterfall
35 driven by tree phenology or natural damage events (e.g. Kato and Onda, 2014; Teramage et al., 2014a;
36 Loffredo et al., 2014, 2015; Itoh et al., 2015; Endo et al., 2015; Okada et al., 2015; Kato et al., 2017,
37 2019; Yoshihara et al., 2016; Nishikiori et al., 2019). These two bio-physical mechanisms gradually
38 transferred the major part of intercepted radiocesium to the forest floor, i.e. up to approximately 80% of
39 the total deposit in less than 3 years, according to at least two distinct ecological half-lives, i.e. about 1
40 month and 10 months (Gonze and Calmon, 2017). These characteristic times were in the range of
41 those measured in forests contaminated by Kyshtym and Chernobyl accidents (e.g. Bunzl et al., 1989;
42 Tikhomirov and Shcheglov, 1991, 1994). At the same time, a small proportion of intercepted
43 radiocesium was absorbed through the leaf surfaces (and to some extent, branch and bark surfaces) then
44 transported in the phloem and xylem notably to the non-directly exposed organs such as root and
45 wood, as well as needles and flowers sprouted after the accident (e.g. Koizumi et al., 2013; Mahara et
46 al., 2014; Masumori et al., 2015; Nishikiori et al., 2015; Kanasashi et al., 2015; Yoshihara et al.,
47 2013, 2014, 2016; Gonze and Calmon, 2017). This “incorporation” process could have started soon
48 after deposition as radiocesium contamination in stem wood and newly expanded plant tissues was
49 already detected at significant levels in 2011 or 2012 (e.g. Tagami et al., 2012; Tanaka et al. 2013;
50 Yoshihara et al., 2013; Kuroda et al., 2013; Ohashi et al., 2014, 2017; Nishikiori et al., 2015; Kajimoto
51 et al., 2015; Kanasashi et al., 2015, 2016; Komatsu et al., 2016). Unfortunately, the respective
52 contributions of foliar and root uptake to the net contamination of stem wood could never be reliably
53 quantified, although some attempts to evaluate it were made at some sites (e.g. Mahara et al., 2014;

54 Nishikiori et al., 2015; Yoschenko et al., 2018). This remains an issue for long-term assessment of
55 radiocesium contamination in timber because the signature of foliar pathways might persist in
56 heartwood over the years. The depuration of tree canopies resulted in a roughly exponential decrease
57 of activity concentration in canopy organs after summer 2011, with an effective half-life typically
58 comprised between 1 and 2 years, depending on the site (Yoshihara et al., 2016; Imamura et al.,
59 2017a; Kato et al., 2017, 2019; Hurtevent et al., in prep). Although they are deemed less important, the
60 contributions of other processes such as incorporation, biomass growth and root uptake in the overall
61 clearance kinetics have still to be evaluated in a quantitative way.

62 During the first few months after deposition, the activity inventory in coniferous forest soils
63 (mainly andosols) remained predominantly trapped in the litter and organic soil, the proportion of
64 activity contained in these horizons being as high as 70% to 90% (Ohno et al., 2012; Koarashi et al.,
65 2012b; Takahashi et al., 2018). After summer 2011, this retention ratio gradually decreased down to
66 less than 25% after few years according to an effective half-life varying between 1 and 3 years,
67 typically (Koarashi et al., 2016a, 2019; Imamura et al, 2017a; Takahashi et al. 2018; Yoschenko et al.,
68 2018; Muto et al., 2019). The variety of mechanisms participating in the downward migration of
69 radiocesium was acknowledged and discussed in several publications (e.g. Fujii et al., 2014; Nakanishi
70 et al., 2014; Koarashi et al., 2016b; Ota et al., 2016; Imamura et al, 2017a; Kurihara et al., 2018; Muto
71 et al., 2019). These included the short-term leaching by rainfall of freshly deposited radiocesium,
72 percolation of solute radiocesium contained in throughfall waters, organic matter degradation and
73 leaching of fine organo-mineral particles. Several studies demonstrated that a greater accumulation
74 and retention of radiocesium occurred in forests with thick organic horizons and dense canopies,
75 because of slower decomposition rates, higher interception of the atmospheric deposit and lasting
76 inputs from tree vegetation (e.g. Koarashi et al. 2012b; Koarashi et al., 2016a; Coppin et al., 2016;
77 Shoko et al., 2017; Takahashi et al. 2018). The situation in Fukushima highly contrasted with
78 observations made in European forests after Chernobyl accident which have consistently shown that a
79 large proportion of radiocesium persisted in the forest-floor organic layers for over a decade (e.g.
80 Schimmack and Bunzl, 1992; Rühm et al., 1996; Strebl et al., 1999; Fesenko et al., 2001; Steiner et al.,

81 2002; Kruyts and Delvaux, 2002; Goor and Thiry, 2004; Konopleva et al., 2009; Thiry et al., 2009;
82 Karadenitz et al., 2015). Several authors invoked the ecological and climatological specificities of
83 Japanese forests such as thinner organic layers, warmer climates, heavier precipitation or other tree
84 species-dependent factors (e.g. Kaneko et al., 2013; Hashimoto et al., 2013; Fujii et al. 2014; Koarashi
85 et al., 2016b, 2019). Due to the strong immobilization of radiocesium leachates in the top mineral
86 profile of Japanese soils (Nakanishi et al., 2014; Koarashi et al., 2016b), the proportion of activity
87 measured after some years below 5 cm depth did not exceed 10%, typically (Koarashi et al., 2012b;
88 Matsunaga et al., 2013; Fujii et al., 2014; Takahashi et al., 2015; Imamura et al., 2017a; Yoschenko et
89 al., 2018). At sites where the soil sampling protocol enabled to demonstrate it, the activity sharply
90 decreased with depth according to a roughly exponential profile, which likely established rapidly and
91 did not drastically changed with years (Koarashi et al., 2012b; Matsunaga et al., 2013; Teramage et al.,
92 2014b, 2016; Takahashi et al., 2015, 2018; Yoschenko et al., 2017; Muto et al. 2019). In parallel, the
93 mobility and bioavailability of radiocesium was shown to strongly decrease with time, especially in
94 the mineral soil, with exchangeable fractions falling to less than 15% in typically one year or less
95 (Koarashi et al., 2012a; Matsunaga et al., 2013; Kang et al., 2017; Manaka et al., 2019). But it is
96 recognized that there are still uncertainties on the role and contribution of the underlying physico-
97 chemical and biological processes involved in the immobilization of radiocesium (Fujii et al., 2014;
98 Teramage et al., 2016; Manaka et al., 2019).

99 The above-mentioned experimental studies considerably improved our understanding of the
100 dissemination processes in forest environments and, not the least, provided a large amount of highly
101 valuable data regarding the short and mid-term consequences of a radiocesium input from the
102 atmosphere. By now, an issue is to which extent the various studies tell the same story, how much is
103 the variability between sites (apart from that inherent to the magnitude of the deposit) and whether it
104 can be explained by site-specific ecological or climatic conditions. Another issue to tackle is whether
105 we can gain further quantitative knowledge from integration of the site-specific data sets, by re-
106 estimating key transfer parameters and elucidating the role or contribution of some of the transfer
107 processes. One particular objective is to re-estimate effective half-lives, mean residence times or

108 transfer rates within the forest system, based on simple mass balance considerations. Another
109 objective is to discuss pending issues concerning, in particular, the impact of (the uncertainty on) the
110 interception fraction upon the activity levels expected in the system, the respective contribution of root
111 uptake and foliar pathways in the contamination of tree organs or the real influence of tree biomass
112 growth upon radiocesium dynamics.

113 To fulfil these objectives, we conducted a detailed review of field data acquired over the period
114 2011-2017 in contaminated Japanese cedar and cypress plantations. The review encompasses 41 forest
115 sites located in the Fukushima and neighbouring prefectures, with a majority of cedar stands planted
116 on andosols. We gathered and analysed hundreds of spatio-temporal measurements of ^{137}Cs activity
117 levels in aerial tree organs (i.e. foliage, branch, stem wood and stem bark) and soil layers (i.e. upper
118 litter, organic layers and mineral soil down to 20 cm depth) as well as measurements of activity
119 depuration fluxes (i.e. litterfall, throughfall and stemflow). The database has been enriched since our
120 previous study (Gonze and Calmon, 2017) because of its extension to the soil component and the years
121 2014-2017. The database further integrates a few new site-specific datasets, including short-term
122 measurements of depuration fluxes published by Nishikiori et al. (2019), as well as some
123 modifications in the preexisting data due to revision by their authors (e.g. Kato et al., 2019). The
124 methodology for processing data as well as the modelling approach for inferring transfer parameters
125 and clarifying processes have both been improved and extended to the soil compartment. In particular,
126 the model includes new transfer processes that can play a role on the mid-term time scales, such as
127 root uptake and tree biomass growth.

128 The present paper organizes as follows. The selected studies and the methodology for
129 processing data are described in sections 2.1 to 2.3. In section 2.4, we describe the conceptual and
130 mathematical approaches used for assessing the transfer of radiocesium within an idealized soil-tree
131 system. In section 3.1, we explore the site-specific observations and discuss their overall consistency
132 and variability. In the remaining sub-sections of section 3, we present and discuss results regarding: (i)
133 the time evolution of the activity partitioning between soil and tree vegetation as a result of
134 interception, depuration and root uptake processes (section 3.2), (ii) the dynamics of activity

135 concentrations in aerial tree organs and the contribution of uptake, incorporation and biomass growth
136 processes (section 3.3), and finally, (iii) the dynamics of activity concentrations in soil layers and its
137 partitioning between layers with a focus on organic matter degradation and downward migration
138 processes (section 3.4). The results are summarized in the conclusion (section 4).

139 1. Material and methods

140 1.1. Selection of field studies

141 In the selection of field studies, the focus was put on researches published in the international or
142 Japanese literature that provided quantitative data on either radiocesium contamination in tree organs,
143 soil layers or depuration fluxes over the period March 2011 - March 2017. The vast majority of more
144 recent data has not yet been published. The focus was put on forest plantations dominated by
145 evergreen coniferous tree species being represented by Japanese cedar (*Cryptomeria japonica*) and
146 Japanese cypress (*Chamaecyparis obtusa*). Forest stands dominated by red pine (*Pinus densiflora*)
147 were also considered in the study of soil contamination because no significant differences with other
148 coniferous soils could be identified. However, radiocesium activity measurements in pine tree organs
149 or collected water and litterfall debris were not included in the dataset because eco-physiological
150 characteristics of pine trees are significantly different from cedar and cypress trees. Mixed forest
151 stands with less than typically 75% of coniferous stems (more than 25 % of broadleaf deciduous trees)
152 were excluded from the review. This implies that, unlike in the meta-analysis conducted by Gonze and
153 Calmon (2017), data acquired for cedar and cypress trees growing in mixed forests were no longer
154 accounted for in the calculation of activity contamination because radiocesium behaviour is likely
155 dependent on the forest type due to notably differences in atmospheric interception and interactions
156 between neighbouring trees. Another important criterion for selecting a site concerned the possibility
157 to estimate the total deposit, based on either the *in situ* measurement of radiocesium inventories in soil
158 and vegetation components or the geographical coordinates. Knowledge of the deposit is of primary
159 importance for normalizing all the radiological quantities and comparing sites.

160 The studies considered in the review are listed in Table 1. They have been pooled into 12
161 groups according to the localization of the forest sites and/or the research institution that conducted
162 monitoring, hereafter named: KATO, YOKO, KAJI, ENDO, NISHI, ITOH, NIIZA, TORI, SHOKO,
163 KOARA, OHNO and KANG. The review encompasses 41 sites referenced in 52 publications, with a
164 majority of 29 cedar sites, 7 cypress, 1 mixed cedar/cypress and 4 red pine sites. Only 3 research
165 groups (KATO, YOKO and KAJI) provided comprehensive measurements of radiocesium
166 contamination in both soil and tree components, while 3 groups (NISHI, ITOH, NIIZA) focused
167 exclusively on depuration processes and 5 groups (TORI, SHOKO, KOARA, OHNO, KANG) focused
168 exclusively on soil. The majority (80%) of the selected forest stands for which age was reported are
169 between 30 and 60 years old while 50% are between 40 and 50 years old. Their mean age is 45 years.

170 To investigate the distribution and behavior of radiocesium in forest vegetation, one sampling
171 strategy consisted in sampling from 3 to 9 trees representative of the forest stand, at most once a year.
172 This experimental protocol which was adopted by KATO, YOKO and KAJI groups to some of their
173 sites enabled to estimate average biomasses (kg d.w. m^{-2}) and radiocesium activity concentrations in
174 standing tree organs ($\text{Bq kg}^{-1} \text{ d.w.}$) – wood, bark, branches, foliage – from which activity inventories
175 in tree vegetation could be evaluated ($\text{Bq m}^{-2} = \text{Bq kg}^{-1} \text{ d.w.} \times \text{kg d.w. m}^{-2}$). This concerned 8 sites.
176 The measurements made by KATO and YOKO groups further distinguished sapwood from
177 heartwood, inner bark from outer bark, small branches from large branches or young needles from old
178 needles (Coppin et al., 2016; Hurtevent et al., in prep; Yoschenko et al., 2017, 2018). Such refined
179 results will not be analysed in the present review. It must be mentioned that only KATO group studied
180 the root system (Coppin et al., 2016; Hurtevent et al., in prep). This first experimental strategy is
181 expected to give estimates of radiocesium contents in tree vegetation that are relatively accurate and
182 representative of the forest stand (on the scale of the plot) as long as the number of sampled trees is
183 sufficient. A complementary approach consisted in monitoring throughfall (*TF*), stemflow (*SF*) or
184 litterfall (*LF*) fluxes ($\text{Bq m}^{-2} \text{ d}^{-1}$), from week to month typically, with the help of water and litterfall
185 collectors conveniently installed below the canopy. This kind of survey was conducted by KATO,
186 YOKO, ENDO, NISHI, NIIZA and ITOH groups. Unlike the previous approach, such experiments

187 further enabled to quantify the time evolution of other important quantities such as water throughfall
188 ($\text{L m}^{-2} \text{d}^{-1}$), biomass fall ($\text{kg d.w. m}^{-2} \text{d}^{-1}$) and activity concentrations in throughfall waters and litterfall
189 debris. Due to a strong small-scale spatial variability induced by the above canopy structure, the
190 estimated fluxes can be very uncertain or biased if the number of collectors is not sufficient or
191 misplaced (e.g. Loffredo et al., 2014, 2015, Zimmermann et al., 2010). Because several of the field
192 studies listed above did not rely on more than typically three collectors (per type of flux), we may
193 expect some inaccuracy in the estimates.

194 At any date, the mean concentration profile in the forest floor ($\text{Bq kg}^{-1} \text{d.w.}$) was estimated at
195 the plot scale by sampling litter and soil layers down to typically 20 cm depth, with a number of soil
196 core samples ranging from 1 to 9 samples, typically. The radiocesium inventory in each layer (Bq m^{-2})
197 was determined by multiplying the activity concentration by the corresponding mass density (kg d.w.
198 m^{-2}). Sometimes, radiocesium activity concentration was below the detection limit in the deeper
199 layers, or simply not investigated below 5 to 10 cm depth at 4 sites (TORI, KANG). For these sites, it
200 is expected that the total inventory in the forest floor cannot be estimated very reliably, especially for
201 late sampling surveys (e.g. 2014 at TORI sites). Generally, the humified layer could not be clearly
202 identified at field or isolated from the fragmented layer. The activity concentration in the litter layer
203 was distinguished from that in the fragmented layer at only 10 sites (Teramage et al., 2014b, 2016;
204 Yoschenko et al., 2017; Coppin et al., 2016; Shoko et al., 2017; Takahashi et al., 2018; Hurtevent et
205 al., in prep). Another difficulty in comparing sites stems from the fact that the vertical slicing adopted
206 for sampling the mineral profile differed from one site to another, or from one survey to another. The
207 finer sampling was carried out by Teramage et al. (2014b, 2016) at the Tochigi cypress site. The
208 coarser samplings distinguished only 3 layers (e.g. 0-5 cm, 5-10 cm and 10-20 cm), which makes it
209 impossible to evaluate the vertical heterogeneity of the radioactivity content in the top few
210 centimetres. The issue of the measurement representativeness is even more acute for soil than for tree
211 vegetation because small-scale spatial variability in soil, initially due to the effect of canopy
212 interception of atmospheric deposition, can be magnified by the natural heterogeneity of the
213 characteristics of the soil layers or magnified by the channelized throughfall/stemflow fluxes (e.g.

214 Takada et al., 2016; Koarashi et al., 2016a; Kang et al., 2017; Kato et al., 2017, 2018; Imamura et al.,
215 2017b; Takahashi et al., 2015, 2018; Muto et al., 2019). As a consequence of small-scale variability in
216 forest medium, the estimation of a mean activity profile can be quite inaccurate.

217 Detailed information regarding the characteristics of the forest sites and sampling strategy is
218 summarized in Table S1 to S12 of the Supplementary Information section S1 where each site is
219 identified by a specific name. Basic ecological characteristics such as the mean tree age (years), the
220 stand density (trees ha⁻¹), the trunk diameter at breast height (cm) or the above ground biomass (kg
221 d.w. m⁻²) were not always stated in the publications. Radiocesium deposit greatly varies among sites,
222 from about 10 kBq m⁻² to more than 1 000 kBq m⁻² in forests located to the north-west of the nuclear
223 site.

224 1.2. Data processing

225 To enable comparison between sites and initiate the analysis, raw monitoring data collected
226 from the above-cited publications required a series of treatments that are briefly detailed herein.

227 Most of the time, activity concentrations in standing vegetation and soil layers estimated at the
228 plot scale were already calculated by the authors as a mass-weighted average over the collected
229 samples. In some publications, a standard deviation was also reported which likely accounted for the
230 variability between samples and/or measurement errors, but calculation details were rarely provided.
231 When individual sample data were reported in the publication, but not the average, we computed the
232 geometric mean (GM) and geometric standard deviation (GSD) including measurement errors if they
233 were stated by the author. Calculations were made through Monte-Carlo simulations based on the
234 assumption of log-normal distributions. The mean activity depuration fluxes were always estimated as
235 the arithmetic mean over the collectors (of identical shape), but the standard deviation was rarely
236 calculated although variability between collectors was important as demonstrated by Loffredo et al.
237 (2014, 2015).

238 1.2.1. *Physical-decay correction to the sampling date*

239 All radiological measurements were decay-corrected to the sampling dates. Physical decay of
240 ^{137}Cs (10972 d half-life) contributed to the decrease of radioactive quantities by only 13% over the 6-
241 year investigation period. However, the influence of physical decay upon radiocesium dynamics in the
242 forest medium increases with the years elapsed after the accident, while foliar transfer and depuration
243 processes that initially dominate over other cycling processes are slowing down dramatically.

244 1.2.2. *Normalization by the deposit*

245 To reduce variability between sites, activity concentrations, inventories and fluxes were
246 normalized by the initial deposit D (decay-corrected to March 15, 2011) estimated at each site (in Bq
247 m^{-2}). Consequently, normalized concentrations and fluxes express in $\text{m}^2 \text{kg}^{-1} \text{d.w.}$ and d^{-1} , respectively,
248 while inventories are unit less numbers. For all sites except those monitored by NISHI and KANG
249 groups, D was estimated based on geostatistical interpolation of the 4th airborne survey measurements
250 (Sanada et al, 2014a,b; NRA, 2017). However, we must keep in mind that the deposit estimates based
251 on airborne surveys may be prone to significant uncertainties (up to tens of percent typically) due to
252 errors in the counting rates, inaccuracy in their conversion into deposit values at the ground level,
253 shielding effects by vegetation or spatial interpolation errors (e.g. Gonze et al., 2014). As reported in
254 Tables S1 to S12 of the Supplementary Information section S1, the calculated values were generally
255 consistent with *in situ* measurements based on the sampling of soil/tree vegetation or the collecting of
256 bulk precipitation. In particular, there is a fairly good agreement at sites where both radiocesium
257 inventories in soil and tree vegetation were measured. We notice a significant discrepancy at only 4
258 sites, with a difference by a factor of 2 at YOKO, SHOKO and OHNO sites, and a factor of 10 at the
259 ENDO site which remains unexplained. In such situations, the highest value was retained. Confidence
260 in the normalized data for ENDO site is accordingly very low. At NISHI and KANG sites, we
261 assumed that the deposit could be approximated by the radiocesium inventory in soil measured in
262 March 2015 and October 2012, respectively. However, the estimates based solely on soil

263 measurements may be quite uncertain due to small-scale spatial heterogeneities induced by tree
264 vegetation.

265 Normalization by the deposit does not suppress all the variability observed between sites. Part
266 of the residual variability is likely due to differences in the atmospheric conditions that prevailed at
267 time of deposition, which in turn caused differences in the interception fraction (denoted f hereafter).
268 The influence of interception upon the distribution of radiocesium within a forest may be significant,
269 especially in the first year after the accident. Unfortunately, the interception fraction remains uncertain
270 at all sites because none of the field studies provided reliable measurements of radiocesium inventories
271 in both soil and tree vegetation immediately after the accident, i.e. in the second half of March 2011.

272 1.2.3. Estimation of the total depuration flux

273 The depuration flux, denoted DF (d^{-1}), was computed from throughfall, stemflow and litterfall
274 fluxes as follows when the three contributions were measured:

275

$$DF = TF + SF + LF \quad (1)$$

276

277 At sites where SF was not measured at a given date, DF was nevertheless estimated based on TF and
278 LF measurements because the contribution of stemflow was about ten times smaller than the 2 others
279 over the 6-year observation period. Unlike in Gonze and Calmon (2017), DF was not estimated from
280 TF alone or LF alone (except when explicitly mentioned) because both contributions played a role
281 after 2012.

282 At KAJI sites, where fluxes were not measured, an annual DF value was nonetheless estimated
283 as the difference between the activity inventories (corrected for physical decay) in soil or tree
284 vegetation over two consecutive years, from Sept. 2011 to Sept. 2015. This approximation justifies as
285 long as we assume that the contribution of root uptake in the soil-tree partitioning of radiocesium can
286 be neglected with respect to that of depuration during this period. As discussed by Gonze and Calmon
287 (2017), it is likely that root uptake indeed remains negligible on the midterm because its characteristic
288 rate of transfer, which is defined as the daily uptake of radiocesium activity per unit surface of soil

289 divided by the total activity inventory in soil, does not exceed a few 10^{-5} d^{-1} (e.g. Linkov and Schell,
 290 1999; Shaw et al., 2003; Hashimoto et al., 2013; Gonze et al., 2015). This characteristic value is
 291 significantly smaller than the typical DF s measured in Japanese coniferous forests in the years
 292 following the accident (see section 2). If the relative contribution of root uptake cannot be neglected
 293 anymore, this calculation method leads to a slight under-estimation of the total depuration flux. The
 294 same approach as that adopted at KAJI sites was used for estimating the annual flux at two of the
 295 KATO sites (e.g. YC and MC sites described in Table S1) based on comprehensive measurements of
 296 activity inventories in Dec. 2013 and Dec. 2014 (Coppin et al., 2016; Hurtevent et al., in prep). DF
 297 could not be straightforwardly estimated at KAJI sites before Sept. 2011 because radiocesium
 298 inventories were not measured before that date. Evaluating a mean DF over this 6-month period (from
 299 March to September) required an assumption on the interception fraction f , as expressed in the
 300 following relationships:

301

$$DF \approx \frac{S_S(t) \times \exp(\lambda^{rad} \times (t - t_0)) - (1 - f)}{(t - t_0)} \approx \frac{f - S_T(t) \times \exp(\lambda^{rad} \times (t - t_0))}{(t - t_0)} \quad (2)$$

302

303 Where $S_S(t)$ and $S_T(t)$ (unitless) are the normalized inventories in soil and tree measured at date t (i.e.
 304 Sept. 1, 2011), t_0 is the date of the main radiocesium fallouts (set to March 15, 2011) and λ^{rad} (d^{-1}) is
 305 the physical decay rate of ^{137}Cs ($\sim 6.32 \cdot 10^{-5} \text{ d}^{-1}$). Because of sampling errors and uncertainty in the
 306 estimated deposit, $(S_S + S_T) \times \exp(\lambda^{rad} \times (t - t_0))$ can significantly differ from its expected theoretical value
 307 of about 1 (between 0.7 and 1.3, typically). This implies that DF estimate depends on whether S_S or S_T
 308 is used; it was decided to take the average value. In accordance with literature, we hypothesized that f
 309 could have varied between 0.70 and 0.90 (Kato et al., 2012; Gonze and Calmon, 2017; Nishikiori et
 310 al., 2019). $DF(f)$ values were estimated for f varying in this range. Although not shown, we
 311 demonstrated that adopting smaller f s led to DF 's estimated at the KAJI sites (based on Eq. 2) which
 312 were definitely too low compared with other sites.

313 1.2.4. Resampling of soil data in depth

314 As the soil sampling procedure differed among sites or surveys (e.g. the slicing of the vertical
315 profile), interpolating data on the same desired horizons was necessary to enable comparison. The
316 discretization chosen for harmonizing data consists of an upper organic layer, without any
317 differentiation between the litter (O_l), fragmented (O_f) and humified (O_h) components, and 3
318 underlying mineral layers down to 20 cm depth, i.e. 0-5 cm, 5-10 cm and 10-20 cm. Adopting a finer
319 discretization by differentiating organic sublayers or exploring mineral profiles at the centimetre scale
320 was not relevant because very few surveys provided that kind of information (see section 1.1).
321 Normalized radiocesium activity inventories (unitless) and mass densities (kg m^{-2}) of each of these
322 four layers were estimated through linear interpolation of raw measurements. This in turn enabled to
323 estimate normalized radiocesium activity concentrations ($\text{m}^2 \text{kg}^{-1}$). When data were partially missing in
324 one of these four layers, due for example to the absence of sampling over the whole layer depth, we
325 did not provide any estimate there.

326 1.2.5. Resampling in time

327 Finally, all normalized radiological quantities were resampled in time in order to provide data at
328 the same frequency, i.e. at the desired constant time step Δt (d). Activity concentrations, inventories
329 and fluxes were re-estimated by log-averaging observations over each resampling period $[t, t+\Delta t]$,
330 starting from the date of the accident (fixed to March 15, 2011). When flux data were partially missing
331 over a period, due for example to a temporary interruption of the monitoring, the value assigned was
332 the average of the existing data. The consequence was that the resampled value of $TF+SF+LF$ could be
333 greater than the resampled value of DF over incomplete periods. Consequently, the time step was kept
334 small enough in order to guarantee an acceptable numerical error. Δt was fixed to 30 days in this
335 study; this value is such that the error (i.e. $TF+SF+LF-DF$) integrated over the observation period did
336 not exceed 1% of the deposit. On the other hand, such a value also preserves the seasonality of flux
337 observations. For activity concentrations in soil layers and tree organs, we further computed a GSD

338 that accounted for raw measurement errors, spatial variability at scales smaller than the forest plot and
339 time variability at scales smaller than the 30-day resampling period

340 1.3. Deriving a “generic” forest stand profile

341 The treatments mentioned above significantly reinforced the consistency between “*site-specific*”
342 observations, due notably to the normalization by the estimated atmospheric deposit. Nevertheless, a
343 significant residual variability persists between sites (within a factor of 5, typically) which likely
344 results from differences in the initial interception of atmospheric radiocesium as well as from
345 differences in the forest stands related to eco-physiological traits, soil properties or climatic
346 characteristics. It must also be stressed that normalized quantities are inherently uncertain because
347 they inherit the uncertainty in the deposit estimate. Another important source of “noise” is the
348 measurement error induced by statistical inaccuracies in the spatially averaged quantities estimated at
349 the scale of the plot. This type of error is expectedly high at sites where too few collectors were
350 installed or too few soil/tree samples were collected at monitoring sites (see Tables S1 to S12 of the SI
351 section for details).

352 It must be acknowledged that a great part of this “variability” or “dispersion” in the data
353 remained poorly understood and was little discussed in the publications. An important barrier to
354 understanding comes from the difficulty to distinguish between natural variability and uncertainty in
355 the measurements or deposit estimates. The lack of systematic knowledge of the initial interception by
356 tree vegetation is another difficulty because it prevents us from analysing radiocesium dynamics based
357 on well-characterised initial conditions. Finally, another important obstacle is the lack of detailed
358 information on some environmental characteristics at some forest sites. Key information or data are
359 often missing because the primary objective of the studies reviewed here was to characterize, as
360 efficiently as possible, the state and dynamics of radioactive contamination in the impacted forests
361 rather than getting a detailed mechanistic understanding of these ecosystems and identifying the
362 reasons behind the variability.

363 In the light of these considerations, we thus propose to assume that all forest stands under study
364 obey more or less the same “*generic*” dynamics within a range of variability/uncertainty of stochastic

365 nature. This mean evolution with time was quantified by log-averaging among sites the radiological
366 quantities derived in section 1.2. The stochastic component was evaluated by calculating a global GSD
367 which accounted for both the site-specific GSD and the variability between sites. Calculations were
368 made through Monte-Carlo simulations based on the assumption of log-normal distributions. Thanks
369 to this method, we computed the time evolution with a 30-day time step of the GM and GSD of the
370 following “*generic*” (or “*mean*”) radiological quantities: throughfall, stemflow, litterfall, total
371 depuration, total inventories in soil and tree, activity concentrations and inventories in the soil layers
372 (organic, 0-5, 5-10, 10-20 cm) and activity concentrations in the tree organs (stem wood, stem bark,
373 branches, foliage).

374 *1.4. Data analysis based on a mass balance considerations*

375 A convenient approach to get a deeper understanding of data is to try to reanalyse them under
376 the light of simple mass budget equations for assessing the redistribution with time of radiocesium
377 fallouts in an idealized soil-tree system. The proposed modelling approach does not aim at explaining
378 or predicting radiocesium dynamics based on a detailed mechanistic description of the various
379 ecological, biochemical and physical processes involved. It is rather intended to check the consistency
380 of the “*generic*” data derived above, based on mass budget considerations and empirical
381 parametrizations of the major transfer processes. Interesting issues are: analysing the coherence
382 between radiocesium activity inventories and depuration fluxes, or checking that the activity
383 concentrations observed in the tree organs, notably foliage, branch and stem wood, can be related to
384 the corresponding inventories through biomasses. A more ambitious objective is to infer some of the
385 transfer parameters by calibrating the model against time observations. Regarding tree vegetation, we
386 are especially interested in estimating a plausible value of the root uptake rate depending on the
387 interception fraction as well as evaluating the respective contributions of foliar and root uptake
388 pathways in the contamination of wood and canopy organs. Regarding the contamination profile in
389 soil, we intend to infer mean residence times for each of the layers considered.

390 1.4.1. Conceptual description of the forest stand

391 As detailed by Gonze and Calmon (2017), our approach for dealing with tree vegetation relies
392 on the assumption that the activity inventory in tree (denoted “ T ”) consists of two well-mixed pools.
393 The so-called “external” pool (“ TE ”) which includes branches, foliage and stem bark, is subjected
394 mainly to interception of atmospheric fallouts and tree depuration. As will be demonstrated later, the
395 contribution of stem bark to the total inventory, biomass and depuration flux is negligible with respect
396 to that of the canopy. As a first approximation, we will neglect bark in the budget. The “internal” pool
397 (“ TF ”) which consists of stem wood and roots becomes increasingly contaminated due in part to
398 incorporation (denoted “ Inc ”) of some proportion of the contamination intercepted by the canopy. The
399 two pools can also be contaminated by root uptake of bioavailable radiocesium (“ Up ”) localized in the
400 rooting soil. Although root uptake may not have contributed significantly in the first few months after
401 initial deposition, its contribution will not be neglected in our analysis, unlike in our previous study.
402 Regarding the rooting soil component (“ S ”), we will assume that it consists of 4 superposed layers, i.e.
403 organic, 0-5 cm, 5-10 cm and 10-20 cm (“ SL ”, “ $S5$ ”, “ $S10$ ”, “ $S20$ ”), each one being characterized by a
404 homogeneous activity concentration (instantaneous mixing assumption). We will assume that the
405 behaviour of radiocesium in soil is governed by depuration from tree, root uptake and “apparent”
406 downward migration (“ F ”) as a net result of the various underlying processes influencing the
407 dissemination of radiocesium in the soil column. Refining the approach by looking into more details to
408 the various biological or physicochemical processes involved in soil is definitely out of scope (e.g.
409 convection, dispersion, organic matter decomposition, sorption/desorption, fixation, immobilization).
410 As depicted in Fig. 1, we thus propose to describe the cycling of deposited radiocesium in the forest
411 stand by considering 6 compartments and 8 transfer processes. At the time scales of interest here, it is
412 reasonable to neglect all other processes susceptible to import/export contamination into/out of the
413 forest stand (e.g. natural tree mortality, management practices, resuspension into the atmosphere, soil
414 erosion, horizontal run-off, drainage to the ground water).

415 1.4.2. Mathematical approach for tree vegetation

416 In accordance with the conceptual model, the time evolution of radiocesium inventories in tree
 417 vegetation obeys the following system of mass balance equations:

418

$$\frac{dS_{TE}}{dt} = f \times \delta(t-t_0) - DF - \underbrace{\lambda^{inc} \times S_{TE}}_{Inc} + \alpha_{TE} \times \underbrace{\lambda^{up} \times S_S}_{Up} - \lambda^{rad} \times S_{TE} \quad (3)$$

$$\frac{dS_{TI}}{dt} = Inc + (1 - \alpha_{TE}) \times Up - \lambda^{rad} \times S_{TI} \quad (4)$$

419

420 Where $S_j(t)$ (unitless) denote the normalized inventories, δ is the Dirac function and DF , Inc and Up
 421 are the normalized net transfer fluxes (d^{-1}) and α_{TE} (unitless) represents the proportion of the root
 422 uptake flux that is allocated to the external organs. For simplicity, we consider here that both
 423 incorporation and root uptake terms are proportional to the inventory in the “upstream” compartment,
 424 with the proportionality factor being the characteristic kinetic rates: λ^{inc} (d^{-1}) and λ^{up} (d^{-1}). These rates
 425 are unknown and controlled by tree physiology as well as the availability of radiocesium in soil for
 426 root uptake. Their values will be assumed constant over the observation period. The allocation
 427 parameter α_{TE} has to be estimated (see below). By summing Eq. 3 and 4, we notice that the rate of
 428 change of the activity inventory in tree, $S_T = S_{TE} + S_{TI}$ (unitless), results from a competition between, on
 429 the one hand, interception and root uptake and, on the other hand, depuration and physical decay.

430

$$\frac{dS_T}{dt} = f \times \delta(t-t_0) + Up - DF - \lambda^{rad} \times S_T \quad (5)$$

431

432 The activity concentrations, $C_{TE}(t)$ and $C_{TI}(t)$ ($m^2 \text{ kg}^{-1} \text{ d.w.}$), can be straightforwardly evaluated from
 433 the corresponding activity inventories based on surface biomasses, $M_{TE}(t)$ and $M_{TI}(t)$ (kg d.w. m^{-2}). We
 434 write:

435

$$C_{TE} = \frac{S_{TE}}{M_{TE}} \quad (6)$$

$$C_{TI} = \frac{S_{TI}}{M_{TI}} \quad (7)$$

436

437 In order to account for biological dilution of intercepted radiocesium over the years, the growth of
 438 forest biomass with age must be taken into account. A relevant approach is to establish “generic”
 439 growth curves that should be as representative as possible of forest plantations located in Fukushima
 440 and neighbouring Prefectures. In accordance to the method adopted by Fukuda et al. (2003), these
 441 growth curves were established by fitting Brody-Mitscherlich equations (e.g. Koya and Goshu, 2013)
 442 to biomass observations collected from the literature for Japanese forest stands between the age of 10
 443 and 60 years. We tested two different models. The first one was proposed by Fukuda et al. (2003)
 444 based on data that were collected for cedar plantations located in Tohoku-Pacific region (Fukushima,
 445 Miyagi and Iwate Prefectures). In the second approach, we re-estimated Brody-Mitscherlich
 446 coefficients based on hundreds of data collected from the literature for both cedar and cypress
 447 plantations located throughout Middle and North Japan, including data already compiled by Fukuda
 448 and co-authors. One reason for testing the two models was the predicted growth rate for canopy
 449 differed quite significantly, especially between the age of 30 and 60 years. For further details, see Fig.
 450 S1 and S2 of the Supplementary Information.

451 One way to estimate the allocation parameter α_{TE} is to assume that radiocesium uptake to tree
 452 compartment j is driven by the net annual primary production NPP_j (kg d.w. $\text{m}^{-2} \text{y}^{-1}$). For the canopy,
 453 NPP is approximately equal to $\Delta M_{TE} + LFM_{TE}$ where ΔM_{TE} (kg d.w. $\text{m}^{-2} \text{y}^{-1}$) is the age-dependent
 454 annual increment of biomass and LFM_{TE} (kg d.w. $\text{m}^{-2} \text{y}^{-1}$) is the age-dependent annual litterfall. The
 455 same rule holds for internal organs except that, in this case, we can neglect biomass losses due to tree
 456 mortality or root turnover. Under this “NPP-based” assumption, the age-dependent parameter $\alpha_{TE}(t)$
 457 writes:

458

$$\alpha_{TE}(t) = \frac{(\Delta M_{TE} + LFM_{TE})}{(\Delta M_{TE} + LFM_{TE}) + \Delta M_{TI}} \quad (8)$$

459

460 As suggested in many research studies (e.g. Sombré et al., 1994; Myttenaere et al., 1993; Goor and
 461 Thiry, 2004; Casadesus et al., 2008; Zhu and Smolders, 2000; Rantavaara et al., 2012; Kobayashi et
 462 al., 2019) an alternative approach is to rely on the assumption that Potassium is a proxy for Caesium.
 463 This means that the partitioning of the root uptake flux is related rather to the net annual demand for
 464 Potassium ($\text{g K m}^{-2} \text{y}^{-1}$), approximately equal to $NPP_j \times [K]_j$ where $[K]_j$ ($\text{g K kg}^{-1} \text{d.w.}$) is the
 465 characteristic K concentration in the newly developed biomass. Under this “K-based” assumption, we
 466 write:

467

$$\alpha_{TE}(t) = \frac{(\Delta M_{TE} + LFM_{TE})}{(\Delta M_{TE} + LFM_{TE}) + \Delta M_{TI} \times [K]_{TI} / [K]_{TE}} \quad (9)$$

468

469 Where the annual biomass increments can be derived from the biomass growth curves while litterfall
 470 and Potassium concentrations must be estimated based on literature data.

471 1.4.3. Mathematical approach for soil

472 According to our conceptual model, the time evolution of activity inventories in soil can be
 473 predicted by the following system of mass balance equations:

$$\frac{dS_{SL}}{dt} = (1-f) \times \delta(t-t_0) + DF(f) - \underbrace{\lambda_{SL} \times S_{SL}}_{F_{SL}} - \alpha_{SL}^{up} \times Up - \lambda^{rad} \times S_{SL} \quad (10)$$

$$\frac{dS_{S5}}{dt} = F_{SL} - \underbrace{\lambda_{S5} \times S_{S5}}_{F_{S5}} - \alpha_{S5}^{up} \times Up - \lambda^{rad} \times S_{S5} \quad (11)$$

$$\frac{dS_{S10}}{dt} = F_{S5} - \underbrace{\lambda_{S10} \times S_{S10}}_{F_{S10}} - \alpha_{S10}^{up} \times Up - \lambda^{rad} \times S_{S10} \quad (12)$$

$$\frac{dS_{S20}}{dt} = F_{S10} - \alpha_{S20}^{up} \times Up - \lambda^{rad} \times S_{S20} \quad (13)$$

474

475 Where λ_j (d^{-1}) represents the apparent migration rate from layer $j=SL, S5$ and $S10$ (i.e. organic, 0-5 and
 476 5-10 cm) to the underlying one, the value of which will be assumed constant over time. These
 477 migration rates can be expressed in terms of residence half-life $\tau_j = Ln(2)/\lambda_j$ (d), which in turn can be
 478 converted into an mean migration velocity, $v_j = h_j/\tau_j$ ($m d^{-1}$) where h_j (m) is the layer's thickness, when
 479 comparing soil horizons of different thicknesses (Frissel and Pennders, 1983; Boone et al., 1985;
 480 Mishra et al., 2018). The parameters α_j^{up} quantify the contribution of each layer to the total root
 481 uptake, with the constraint that $\sum \alpha_j^{up} = 1$. It will be demonstrated in section 2.4 that root uptake has
 482 little influence upon the dynamics of activity inventories in soil over the observation period with
 483 respect to depuration and downward migration. This, in turn, implies that the assumption made on the
 484 uptake partitioning between layers does not play a significant role in the calculations. Accordingly, we
 485 will assume for simplicity that $\alpha_j^{up} = S_j/S_S$, where $S_S = S_{SL} + S_{S5} + S_{S10} + S_{S20}$ (unitless) is the total inventory in
 486 soil. By summing Eq. 10 to 13, we notice that the rate of change of the activity inventory in soil
 487 writes:

488

$$\frac{dS_S}{dt} = (1-f) \times \delta(t-t_0) + DF(f) - Up - \lambda^{rad} \times S_S \quad (14)$$

489

490 The activity concentration $C_j(t)$ ($m^2 kg^{-1} d.w.$) in any soil layer $j=SL, S5, S10$ and $S20$ can be
 491 calculated from the corresponding activity inventory based on its mass density, M_j ($kg d.w. m^{-2}$):

492

$$C_j = \frac{S_j}{M_j} \quad (15)$$

493

494 For the mineral layers, M_j can be further expressed in terms of the bulk soil density ρ_j (kg d.w. m⁻³)
495 and the layer's thickness h_j (m). The mass densities were estimated by compiling their values
496 measured at the dozens of selected sites.

497 1.4.4. Inferring transfer rates

498 As mentioned above, one motivation behind the use of such a dynamic model was to estimate
499 plausible ranges of variation of the unknown transfer parameters – λ^{up} , λ^{inc} and λ_j – for varying values
500 of f (i.e. 0.70, 0.75, 0.80 and 0.85). This was accomplished by adjusting the predicted activity
501 inventories and concentrations to their observed “generic” values over the 6-y period, while fixing
502 $DF(f)$ to its observed “generic” value. Calibration of the root uptake rate λ^{up} was accomplished by
503 minimizing the RMS errors on the logarithmic values of S_T and S_S (Eq. 5 and 14), where the errors
504 were normalized by the observed Geometric Standard Deviations (GSDs) to account for uncertainties
505 in the observations. Relying on the best estimate of λ^{up} , the incorporation rate λ^{inc} was then estimated
506 by adjusting the calculated logarithmic values of C_{TE} and C_{TI} (Eq. 3, 4, 6, 7 and 8 or 9) to the measured
507 ones. In this second stage, we took into account: (i) the uncertainties associated to the stand age at the
508 date of deposition by randomly varying it between 30 and 60 years, (ii) the imprecision in the biomass
509 growth by randomly selecting one growth model over the other, and (iii) the uncertainties in litterfall
510 and K concentration ratio based on a literature review. Finally, the apparent migration rates λ_j were
511 estimated successively from the surface to the bottom layer, by adjusting the log-values of both S_j and
512 C_j (Eq. 10 to 13 and 14) to the measured ones (i.e. minimizing the sum of both MSLEs). The
513 adjustment was performed for each best estimate of λ^{up} and λ^{inc} , despite the fact that they have very
514 little influence upon the solution. In addition to the uncertainties mentioned above, the uncertainty in
515 the soil densities was further introduced here as it strongly influences activity concentrations in soil.
516 All calculations relied on Monte-Carlo techniques.

517 2. Results and discussion

518 2.1. Overview of site-specific observations

519 In this section, we briefly present the site-specific observations and discuss their general trends
520 without going into details for a specific site because these results were already discussed by each
521 research group.

522 The time measurements of the normalized activity inventories in soil (S_S) and tree vegetation
523 (S_T) at sites where both quantities were investigated (5 KAJI, 1 YOKO and 2 KATO sites) are
524 displayed in Fig. 2. The first reliable characterization of radiocesium distribution in Fukushima forests
525 did start in late summer 2011, thanks to surveys at 4 KAJI sites. Due to sampling inaccuracy and
526 uncertainty in the estimated deposit, the total activity inventory S_S+S_T corrected for the physical decay
527 (not shown) is not necessarily equal to 1. Indeed, the set of 33 data collected from Sept. 2011 to Dec.
528 2016 leads to total values ranging between 0.70 and 1.38. Despite the dispersion observed, the data
529 suggest that less than 10% of the initial deposit remained in tree vegetation after 3 years, while more
530 than 80% was recovered in the forest floor, due notably to depuration processes (13% being lost by
531 physical decay)

532 The concurrent evolution of the activity depuration flux measured at 14 different sites is
533 depicted in Fig. 3. When available, the corresponding time observations of TF , SF and LF are
534 provided in Fig. S3. The dataset was modified or enriched with respect to that published by Gonze and
535 Calmon (2017) as it relies on data updated by Kato et al. (2019) over the period 2011-2013 at 2 pre-
536 existing sites (e.g. KATO sites) and includes a few new sites (e.g. 1 KAJI, 1 YOKO, 1 NIIZA and 4
537 NISHI sites). It is also more reliable because DF was estimated considering both TF and LF and
538 because anomalous LF data reported before June 2011 at the KATO_TO-Cy site were excluded from
539 the dataset (cf. discussion in Calmon et al., 2015). A rather satisfactory consistency exists between the
540 various time series that typically fall within a factor of 10. Part of the variability observed in
541 Fukushima forests was shown to be driven by spatial variations or time fluctuations in climatic and
542 eco-physiological processes, mainly rainfall and biomass litterfall (e.g. Hisadome et al., 2013;
543 Loffredo et al., 2014; Endo et al., 2015; Okada et al., 2015; Yoshihara et al., 2016; Kato et al., 2017;

544 Gonze and Calmon, 2017). As depicted in Fig. 3, the depuration flux drastically decreased by about 2
545 orders of magnitude in 6 years, according to roughly two kinetics: an initial fast decrease in 2011
546 followed by a slower decrease over the remaining years. The initial decrease of DF mainly resulted
547 from the decrease of throughfall contribution that initially dominated, while litterfall contribution
548 became increasingly important on the longer term (Fig. S3). Despite the lack of data, one can observe
549 that stemflow remained negligible over the 6-y period and smaller than other contributions by a factor
550 of 10, typically.

551 Activity concentrations in needles and stem wood are given in Fig. 4 (see Fig. S4 for stem bark
552 and branches). The dataset consists of 70 data for foliage and 35 data for stem wood based on 9
553 different sites. The variability between sites is mostly within a factor of 5 to 10 for all tree organs, but
554 seemingly increases with time for needles. From summer 2011, the activity in foliage rapidly
555 decreased over the observation period by at least a factor of 10, while the activity in stem wood seems
556 to have slightly increased over the same period. However, the trend analysis in stem wood is made
557 difficult due to the large range of variation between sites. As field monitoring of tree organs did not
558 start before the end of July 2011, none of the surveys provided information regarding the short-term
559 redistribution of intercepted radiocesium within vegetation. We cannot exclude that, during the first
560 few months, radiocesium activity in foliage might have decreased more rapidly than observed after,
561 because of a very high throughfall flux during that short-term period. In the same way, activity
562 concentrations in stem wood might have rapidly increased on this short-term period according to a
563 characteristic time which remains uncertain (ranging from days to months).

564 As depicted in Fig. 5, the activity concentrations in the 4 soil layers are rather well
565 differentiated, notably between the upper organic and the lower 0-5 and 5-10 cm mineral layers, with
566 nearly an order of magnitude difference between 2 consecutive layers. The dataset, which gathers
567 about 80 data per horizon, reveals a strong consistency between the 23 forest sites, notably in the first
568 two layers where the values remain confined within a factor of 5, typically. The residual dispersion
569 seems to increase with decreasing activity concentrations in depth. The picture further reveals distinct
570 trends over time. While the activity concentration in the organic layer continuously decreased from

571 summer 2011 to winter 2016, by about a factor of 5, the radioactive levels in the 3 mineral layers
572 concomitantly increased, according to kinetics that look very similar. Like in tree vegetation, we may
573 regret the quasi absence of measurements before mid-June 2011; the only available data is that
574 provided by OHNO group in mid-April at a site where the estimated deposit is rather uncertain (a
575 factor of 2 between the *in situ* and airborne values).

576 2.2. Generic soil-tree partitioning and depuration processes

577 The time evolutions of the total activity inventories in soil and tree vegetation are displayed in
578 Fig. 6, in conjunction with the time history of the mean activity depuration flux and its time integrated
579 value in Fig. 7 for $f=0.85$. The grey portions in Fig. 7 indicate periods when either throughfall or
580 litterfall was missing, in which case DF was estimated from TF or LF alone. The increase of
581 radiocesium inventory in soil, which mainly resulted from the depuration of contaminated canopies,
582 took place in at least two distinct stages, i.e. an initial rapid increase followed by a slowing down after
583 the autumn 2012, in accordance with the kinetics of the depuration flux. The total depuration flux
584 decreased by 2 orders of magnitude in only 4 years, from an initial rate of about 0.5% per day during
585 the first few weeks to about 0.05% after only 1 year and about 0.005% after 4 years. As indicated in
586 Fig. 7, we estimate that, on average, about 80% of the initial deposit was transferred to the forest floor
587 due to depuration over the whole 6-year period (with $f=0.85$) while about 5% was left in tree
588 vegetation. This characteristic time of transfer is longer than that derived in our previous meta-analysis
589 where we estimated that the same amount had already returned to soil in only 3 years (with $f=0.90$).
590 The influence of root uptake upon radiocesium partitioning between soil and tree vegetation was likely
591 little in the very first few years after the accident (e.g. Nishikiori et al., 2015; Yoshihara et al., 2016)
592 although we cannot exclude that root transfer might have started to counterbalance depuration at the
593 end of the observation period. Another interesting question is to examine the consistency between
594 inventory and depuration measurements, as well as the influence of the chosen value of f upon the
595 results. A convenient approach to explore these issues is to use the simple dynamic model introduced
596 in section 1.4. The calculated RMSE on the predicted S_T and S_S inventories (i.e. partitioning) is
597 depicted in Fig. S7a for varying interception fractions. The simulations clearly indicate that, in order to

598 be consistent with measurements, the contribution of the root uptake can no longer be neglected as
599 long as we assume an interception fraction smaller than 0.85, typically. The best-estimated values of
600 the root uptake for varying f 's are given in Table 2. The lowest RMSE was obtained for $f=0.70$ and
601 $\lambda^{up}=3.9 \cdot 10^{-5} \text{ d}^{-1}$, in which case the predicted activity levels are mostly within the observation ranges as
602 shown in Fig. 6. Comparing these results with those obtained by imposing $\lambda^{up}=0 \text{ d}^{-1}$ (not shown)
603 suggests that, for such an interception fraction, root uptake might have been responsible for the
604 increase of the activity content in tree vegetation by about 5% of the initial deposit after 6 years.
605 Another satisfactory agreement between predicted and observed values, however, was obtained for
606 $f=0.85$ and a quasi-nil root uptake ($\lambda^{up}<1 \cdot 10^{-6} \text{ d}^{-1}$). As shown in Fig. 6, this leads to quite comparable
607 results over the last 3 years. It is difficult to infer from this analysis whether root uptake played a role
608 or not because the uncertainty on the interception fraction remains. Yoschenko et al. (2018) attempted
609 to estimate the contribution of root uptake to the contamination of the aboveground vegetation, based
610 on a simple mass balance analysis of inventory data acquired in their Japanese cedar stand. Although
611 they recognize that their estimate is highly uncertain, they indicate that root uptake might have
612 contributed to an annual increase of S_T between 0.3% (in 2014) and 2% (in 2015) of the total inventory
613 present in the system. It can be easily checked that these values are consistent with our own estimation
614 based on the values of λ^{up} derived above, which would lead to an annual root uptake varying between
615 $\sim 0\%$ ($f=0.85$) and 1.2 % ($f=0.7$) over the same period. On the short term, none of the simulations fits
616 well with data: when the prediction in soil is improved, it is deteriorated in tree vegetation, and *vice*
617 *versa*. Whatever the parameter values, this mass balance model is not able to explain the observations
618 because it inevitably predicts in Sept. 2011 a total activity inventory which is close to one (0.99, in
619 accordance with physical decay) while the mean observed value is significantly smaller (0.79). Such a
620 low value would imply that a substantial proportion of the radiocesium deposit ($\sim 20\%$) had already
621 disappeared from all the forest stands after only 6 months due to a dramatic export by soil erosion or
622 run-off. Rather it is more reasonable to point to the inaccuracies in the measurements that are likely to
623 explain the underestimation of the activity inventory in 2011, and conversely, its overestimation in
624 Sept. 2015.

625 The respective contributions of TF , LF and SF fluxes and their cumulative values are compared
626 in Fig. 8. These values were derived by only considering sites where both throughfall and litterfall
627 components were measured. The dozen of ITOH sites that were not equipped with litterfall samplers
628 were excluded here because they generally exhibited throughfall values significantly greater than those
629 reported at other sites (*cf.* Fig. S3). Because these sites account for half of the sites where throughfall
630 was measured on the very short term, considering them would have induced a considerable bias by
631 artificially boosting the relative contribution of TF , notably with respect to LF (for further details, see
632 Gonze and Calmon, 2017). As already discussed in previous researches (e.g. Schimmack et al., 1993;
633 Loffredo et al., 2014; Endo et al. 2015; Okada et al. 2015; Yoshihara et al., 2016; Gonze and Calmon,
634 2017; Kato et al., 2019; Nishikiori et al. 2019), the time variability of TF was shown to be in part
635 driven by that of precipitation, or leaching of radioactive and stable Cesium from internal plant tissues
636 (Nishikiori et al. 2019), while the time variability of LF was essentially attributed to that of the
637 biomass fall. We notice in Fig. 8b that litterfall is characterized by a strong seasonal behaviour with
638 approximately two characteristic peaks: a strong systematic peak in the autumn and another one in the
639 early spring when needles are sprouting (March-April). This seasonality in litterfall induces peak-to-
640 valley differences by a factor of 5, typically. The data confirm that TF decreased by 2 orders of
641 magnitude in only 2 years, while LF decreased by only one order of magnitude in 6 years. Such a
642 difference in the magnitude of their decreases can only be explained if we differentiate at least two
643 kinds of radiocesium pools in the canopy: a “leachable” pool corresponding to a residual fraction of
644 the radiocesium initially intercepted by canopy surfaces (e.g. needles cuticle, outer bark of branches
645 and twigs) and a “non-leachable” pool corresponding to the remaining fraction which has been
646 incorporated into canopy internal tissues through foliage cuticle or immobilized onto the branch bark.
647 According to this schema, throughfall process corresponds to the leaching of the “leachable”
648 contamination by rainfall while litterfall corresponds to the loss of both contamination pools through
649 biomass fall. Because the two loss processes affect the leachable pool, it is more rapidly depleted than
650 the other one. This in turn might explain why throughfall decreases more rapidly than litterfall. The
651 incorporation of radiocesium into the internal tissues may exacerbate this difference, as this

652 mechanism tends to deplete even more the leachable fraction. Our analysis further demonstrates that
653 *TF* strongly dominated during the first few months and induced a tree-to-soil transfer of contamination
654 equal to ~48% of the deposit after only one year, while *LF* and *SF* contributed ~7% and less than 1%,
655 respectively. During the three following years (from March 2012 to March 2015), the trend was
656 reversed, as we notice that the cumulated litterfall amounted to ~10% while throughfall contributed
657 ~6%. It is difficult to draw conclusions after June 2015 because the data which rely on only 2 sites
658 (e.g. YC and MC sites monitored by KATO group) are partially missing and strongly variable. An
659 attempt to extrapolate the cumulated fluxes until March 2017 is made by assuming a zero flux over the
660 periods where measurements were lacking. Under this slightly underestimating hypothesis, the final
661 contributions of throughfall, litterfall and stemflow at the end of the 6-year period amount to ~56%,
662 ~22% and ~1% of the deposit, respectively. The throughfall process thus contributed more than two
663 thirds of the return-to-soil transfer of radiocesium activity while litterfall contributed less than one
664 third. The total amount of radioactivity transferred to the forest floor in 6 years is thus estimated to
665 about 79%; this is consistent with the value of 80% deduced from the total depuration flux.

666 2.3. Generic activity concentrations in tree vegetation

667 The time evolutions of the *mean* radiocesium activity concentrations in tree organs are
668 displayed in Fig. 9. From June 2011 to Dec. 2016 (5.5 years), the activity concentrations in needles
669 and branches decreased by a factor of 18 and 10, respectively, while it decreased by a factor of only
670 1.6 in stem bark. In a first approximation, we can assume that the decrease in these 3 compartments
671 was exponential over this period with effective decay rates (physical decay included) equal to
672 respectively $0.50 \pm 0.08 \text{ y}^{-1}$, $0.39 \pm 0.03 \text{ y}^{-1}$ and $0.06 \pm 0.02 \text{ y}^{-1}$ (i.e. effective half-lives equal to about 1.4
673 y, 1.8 y and 11.5 y). The adjustment was accomplished by minimizing the RMSE of the logarithmic
674 values of the activity concentrations (normalized by their respective GSDs). The effective decay rate
675 of 0.50 y^{-1} calculated for needles is in the range established by Imamura et al. (2017a) based on Sep.
676 2011 – Sep. 2015 measurements at their 5 coniferous forest sites, i.e. $0.45 - 0.88 \text{ y}^{-1}$ with an arithmetic
677 mean of 0.68 y^{-1} . Our estimate is also consistent with the decay rates calculated by Hurtevent et al. (in
678 prep.), $0.47 \pm 0.04 \text{ y}^{-1}$ and $0.48 \pm 0.08 \text{ y}^{-1}$, based on field surveys conducted from Dec. 2013 to Dec. 2018

679 at two of the KATO sites (i.e. YC and MC). The values established by Kato et al. (2019) at the same
680 two sites, based on their own measurements conducted from Jul. 2011 to Dec. 2016, amounted to
681 respectively 0.26 y^{-1} and 0.40 y^{-1} for old needles, and 0.55 y^{-1} and 0.54 y^{-1} for new (annual) needles.
682 The mean values for the whole foliage were not estimated by the authors but are inevitably in the
683 range $0.26 - 0.55 \text{ y}^{-1}$ (YC) and $0.40 - 0.54 \text{ y}^{-1}$ (MC). The smaller values estimated by Kato and co-
684 authors may result from the fact that the activity levels measured from late 2014 to late 2016 in
685 needles were significantly higher than those measured by Hurtevent and co-authors (by a factor of 2
686 typically); this led to a lower estimate of the decay slope. Another possible reason is that both
687 experimental protocols and observation periods differed between the two studies, which may have
688 resulted in different estimates. The effective decay rate in branches which amounts to 0.39 y^{-1} is quite
689 consistent with the values estimated by Imamura et al. (2017a), between 0.41 y^{-1} and 0.53 y^{-1}
690 (arithmetic mean of 0.46 y^{-1}), or those established by Hurtevent et al. (in prep.) at the YC and MC
691 sites, i.e. $0.48 \pm 0.03 \text{ y}^{-1}$ and $0.36 \pm 0.10 \text{ y}^{-1}$, respectively. The difference in the decay rate with needles is
692 statistically significant although moderate. The mean estimate of 0.06 y^{-1} in bark is in the range of
693 values estimated by Kato et al. (2019), between -0.094 and 0.20 y^{-1} , based on data published by
694 Imamura et al. (2017a) for their cedar sites. It also falls in the range provided by Kato et al. (2019)
695 based on 4-y observations (2013-2016) at the YC and MC sites, i.e. $-0.04 - 0.10 \text{ y}^{-1}$. However, the
696 latter comparison is not straightforward because the estimate here was based on measurements of ^{137}Cs
697 concentration in the outer bark and thus could differ from those established for the whole bark. For the
698 same two sites, Hurtevent et al. (in prep.) estimated these rates over the period 2013-2018 to
699 respectively $0.16 \pm 0.02 \text{ y}^{-1}$ and $0.22 \pm 0.04 \text{ y}^{-1}$ for the whole bark. The estimates of the effective decay
700 rates in stem bark are highly variable and uncertain because the observation periods that do not exceed
701 5 years are probably too short for accurately estimating such long half-lives, i.e. the magnitude of the
702 measurement errors are typically greater than the mean decrease over the period.

703 The decrease of activity concentrations in canopy organs can be compared with that of
704 radiocesium inventory in aerial tree vegetation. As indicated in Fig. 9, the activity inventory in tree
705 decreased according to an effective half-life of about 2.1 y that is significantly longer than that

706 estimated in the canopy. This enhanced decrease is likely caused by the combined effects of: (i)
707 biological dilution of the intercepted ^{137}Cs activity induced by the growth of canopy biomass and (ii)
708 incorporation of an increasing proportion of ^{137}Cs activity into internal organs that were not directly
709 exposed to atmospheric fallouts, i.e. inner bark, sapwood, heartwood and root system. Biological
710 dilution alone cannot explain the difference because it does not exceed a few percent per year for the
711 coniferous tree species considered in this study (Cf. Fig. S2). The internalization and translocation of
712 intercepted radiocesium have certainly contributed to the contamination of wood, already detected in
713 summer 2011. The importance of the foliar pathway in the contamination of internal organs, especially
714 stem wood, was already highlighted by several field studies conducted in Japanese forests (e.g.
715 Kuroda et al., 2013; Mahara et al., 2014; Ohashi et al., 2014; Nishikiori et al., 2015; Komatsu et al.,
716 2016; Wang et al., 2016; Hara et al., 2020).

717 To gain further insights into our understanding of the mechanisms driving the activity
718 concentrations in tree organs, we can come back to mass budget considerations. One issue is to check
719 whether the compartmental model can explain (reproduce) the rapid decrease of activity
720 concentrations in the canopy organs, due to the combined effect of depuration, incorporation, biomass
721 growth and physical decay. A second issue is to evaluate to what extent foliar incorporation of the
722 intercepted radiocesium contributed to the contamination of wood. As detailed in section 1.4.4, the
723 proposed method consists in estimating a plausible value of the incorporation rate by calibrating
724 against data the activity concentrations predicted in the two tree pools. First, to enable the calculation
725 of the allocation factor α_{TE} (Eq. 8 and 9), it was necessary to estimate the biomass litterfall LFM as
726 well as the concentration ratio $[K]_{TI} / [K]_{TE}$ required in the K-based approach. The biomass litterfall
727 was essentially monitored at the KATO and NISHI forest sites, from March 2011 to March 2015.
728 After that period, data were reported for only 2 sites. Following a methodology similar to that
729 described for radiocesium data, we derived a “generic” value of LFM in Fig. S5. Its time evolution is
730 characterized by a strong seasonality with 2 remarkable annual peaks, a first one in early spring and a
731 second one in the autumn season. The mean annual value calculated over this 4-yr period amounts to
732 $0.51 \text{ kg d.w. m}^{-2} \text{ y}^{-1}$ ($1.4 \text{ g m}^{-2} \text{ d}^{-1}$). This value agrees satisfactorily with those generally reported in

733 mature Japanese cedar and cypress forests (e.g. Haibara & Aiba, 1982; Katsuno et al., 1984; Katigiri et
 734 al., 1990; Nakane, 1995; Kaneko et al., 1997; Miura, 2000; Ichikawa et al., 2003a,b; Shutou &
 735 Nakane, 2004; Yamashita et al., 2004; Yoshida & Hijii, 2006; Inagaki et al., 2010a,b, 2012; Miyamoto
 736 et al., 2013; Wang et al., 2016). Among the dozens of sites investigated by these authors, the annual
 737 litterfall varies in the range $0.53 \pm 0.15 \text{ kg d.w. m}^{-2} \text{ y}^{-1}$ (mean \pm SD). The canopy was shown to
 738 contribute about 80% in the litterfall. Accordingly, we imposed $LFM=0.41 \pm 0.12 \text{ kg d.w. m}^{-2} \text{ y}^{-1}$ in the
 739 calculations. For a 45-yr old forest stand, the biomass growth curves depicted in Fig. S1 give annual
 740 biomass increments, ΔM , equal to approximately $0.42 \text{ kg d.w. m}^{-2} \text{ y}^{-1}$ for the internal organs and
 741 $<0.07 \text{ kg d.w. m}^{-2} \text{ y}^{-1}$ for the external organs. If we adopt the NPP-based approach, this leads to an
 742 allocation factor $\alpha_{TE} \sim 52\%$. If we rely rather on the K-based approach, the proportion of radiocesium
 743 allocated to the canopy is increased because K concentration is generally greater in foliage than in
 744 stem wood. The wood-to-canopy K concentration ratio typically ranges between 0.2 and 0.5 (e.g.
 745 Ohrui and Mitchell, 1996; Wang et al., 2016; Nagakura et al., 2017; Iizuka et al., 2018; Hurtevent et
 746 al., in prep.). Consequently, with this second approach, the value of α_{TE} is increased between 67% and
 747 85%. Accordingly, we adopted in the model a wood-to-canopy K concentration ratio randomly varied
 748 between 0.2 (highest α_{TE} with the K-based approach) and 1 (lowest α_{TE} with the NPP-based approach).
 749 As summarized in Table 2, the calibration simulations indicate that the best-estimated value of the
 750 incorporation rate λ^{inc} ranges between $5 \cdot 10^{-5}$ and $6 \cdot 10^{-5} \text{ d}^{-1}$, depending on the chosen interception
 751 fraction. This transfer rate was easily identifiable for high interception fractions ($f \geq 0.80$) due to a
 752 pronounced minimum of the error in this range (see Fig. S7b). The activity concentrations predicted in
 753 tree vegetation based on the best-estimated values of the incorporation and root uptake rates are
 754 compared to observations in Fig. 10 for $f=0.70$ and 0.85 . Both simulation results satisfactorily agree
 755 with observations, including on the short term. Activity concentrations predicted in the external (resp.
 756 internal) organs seem slightly better with $f=0.70$ (resp. 0.85). According to the model, the mean
 757 activity concentration that is expected in the canopy immediately after deposition is equal to fM_{TE} . For
 758 a 45-yr old forest stand, the growth models give a canopy biomass of approximately 4 kg d.w. m^{-2} ,
 759 thereby giving an initial activity concentration between 0.17 and $0.21 \text{ m}^2 \text{ kg}^{-1} \text{ d.w}$ for the range of

760 interception fractions considered. We may further notice that the decrease of the activity concentration
761 in the canopy progressively slows down until summer 2012 according to a time-varying characteristic
762 rate (i.e. the decrease is not exponential). After summer 2012, the decay slope is stabilizing at a
763 constant rate of about 0.48 y^{-1} , in-between the effective decay rates estimated above for branches and
764 needles (0.39 y^{-1} and 0.50 y^{-1} , respectively). Although not shown, the calculations suggest that,
765 whatever interception fraction is, canopy depuration contributes to about 95% of the total decrease in 6
766 years, while incorporation, physical decay and biological dilution accounts respectively for 2%, 2%
767 and 1%. With $f=0.70$, the simulations further indicate that incorporation contributes to about 40% of
768 the activity transferred to internal organs after 6 years (100% for $f=0.85$), the remaining 60% being
769 induced by root uptake. Although not shown, the calculations suggest that the influence of root uptake
770 starts at the earliest after 2 years. Unfortunately, we must recognize that the challenge remains to infer
771 a more precise value of the interception fraction and decide among the various scenarios, based on this
772 mass balance analysis.

773 2.4. Generic activity concentrations and inventories in soil

774 Time evolution of the *mean* radiocesium activity concentrations measured in soil layers from
775 April 2011 to Dec. 2016 is given in Fig. 11. The corresponding evolution of the activity inventory is
776 depicted in Fig. S6. The best-estimate model outputs are also shown in the figures; they will be
777 discussed later.

778 Despite some dispersion in 2011, the data suggest a peak in the organic layer's activity of about
779 $0.5 \text{ m}^2 \text{ kg}^{-1} \text{ d.w.}$ in summer 2011. We notice that this is more than two times greater than that
780 estimated in tree canopy immediately after deposition (between 0.17 and $0.21 \text{ m}^2 \text{ kg}^{-1} \text{ d.w.}$).
781 Theoretically, this peak is reached when the (decreasing) depuration flux becomes balanced by the
782 (increasing) output migration flux down to the top mineral layer, i.e. when $DF \approx \lambda_{SL} \times M_{SL} \times C_{SL}$ where
783 $\lambda_{SL} \text{ (d}^{-1}\text{)}$ is the apparent migration rate introduced in section 1.4.3. After summer 2011, the activity
784 concentration in the organic layer decreased by a factor of about 6 in 5.5 years, according to a roughly
785 exponential decay rate of $0.32 \pm 0.05 \text{ y}^{-1}$. This corresponds to an effective half-life of about 2.2 y, in the
786 midst of the range of values estimated at a few sites and typically comprised between 1 to 3 years

787 (Koarashi et al., 2016a, 2019; Imamura et al, 2017a; Takahashi et al. 2018). The activity inventory
788 followed a similar trend because these two quantities are related to each other by the mass density,
789 which in a first approximation remained constant over the observation period. The mass of the organic
790 layer was either reported or deducible from concomitant S_{SL} and C_{SL} measurements (cf. Eq. 15) at 25
791 forest sites (cf. Tab. 1). Time measurements did not show any drift at any selected site but some
792 “noise” attributed to sampling uncertainties and natural variability of biomass litterfall, OM
793 decomposition rate or climatic conditions. The mean value was estimated to $1.9 \pm 0.3 \text{ kg d.w. m}^{-2}$ ([1.1–
794 2.9]). The statistics include measurements at all sites and over time at same sites. Using the measured
795 value of $DF(f)$ in summer 2011, it is now possible to estimate the apparent migration rate down to the
796 mineral soil based on the above-mentioned relationship. For $f=0.85$, we get: $\lambda_{SL} \sim 1.5 \cdot 10^{-3} \text{ d}^{-1}$. This
797 corresponds to a mean residence time equal to about 1.3 year in the upper organic layer. A more
798 accurate estimation will be provided below through model calibration.

799 Downward migration of radiocesium increased the contamination levels in all mineral soils,
800 with a seemingly more pronounced effect during the first year as already noticed in some soil studies
801 (e.g. Matsunaga et al., 2013; Koarashi et al., 2016b; Imamura et al., 2017a; Muto et al., 2019). The
802 variety of mechanisms contributing to migration was discussed in several publications (e.g. Fujii et al.,
803 2014; Nakanishi et al., 2014; Koarashi et al., 2016b; Ota et al., 2016; Imamura et al, 2017a; Muto et
804 al., 2019). These mechanisms include the leaching by rainfall of freshly deposited radiocesium,
805 percolation of solute radiocesium contained in throughfall waters, organic matter degradation and
806 leaching of fine organo-mineral particles. The rapid initial increase of radiocesium activity in the
807 mineral soil suggest that some proportion of freshly deposited radiocesium, not yet immobilized by
808 biological or physico-chemical processes, rapidly migrated to the very top mineral layer. Percolation
809 of contaminated throughfall waters must have also contributed because radiocesium returning to the
810 forest floor during this early period was essentially driven by throughfall and supposedly in a
811 relatively mobile physico-chemical form, unlike that trapped in the litterfall debris (e.g. Teramage et
812 al., 2018, 2019a,b). After summer 2011, the contamination levels continued to increase more slowly in
813 all mineral horizons, the activity level in the top 5 cm layer remaining an order of magnitude higher

814 than that in the 5-10 cm layer. Such a high activity level in the top mineral layer was ascribed to the
815 strong immobilization of radiocesium leachates from the organic layers in the very first centimetres
816 (Nakanishi et al., 2014; Koarashi et al., 2016b). Several laboratory studies conducted on Fukushima
817 forest soils further demonstrated that the proportion of exchangeable (supposedly mobile) radiocesium
818 in organic and mineral soil rapidly dropped down to less than 25% in a few months (Matsunaga et al.,
819 2013; Saito et al., 2014; Manaka et al., 2019). The rapid decrease of radiocesium availability and
820 mobility is responsible for the slowing down of the dynamics. Manaka et al. (2019) demonstrated that
821 the proportion of exchangeable radiocesium in the top 5 cm mineral layer at one of their coniferous
822 sites (KAJI sites) was about half that measured in the organic layer. The higher availability of
823 radiocesium in organic soil was ascribed to a lower amount of silt- and clay-sized particles or the
824 inhibition by well-decomposed organic matter of radiocesium adsorption on clay minerals (Koarashi et
825 al., 2012b; Mishra 2018). Going back to Fig. 11 and S6, we notice that the time evolutions of the
826 activity concentration and inventory in any layer j ($S5$, $S10$ and $S20$) are nearly parallel (in a log y
827 axis) because both quantities are linked by the dry bulk density ρ_j that are roughly constant over time
828 (see below).

829 Looking at the partitioning of radiocesium inventory between the four layers is also informative.
830 As demonstrated in Fig. 12, more than 50% of the inventory was already present in the mineral soil
831 after 2 years or less, with a significant proportion – between 5% and 10% – already moved below 5
832 cm depth. This is in reasonable agreement with observations made at several coniferous forest sites
833 (Koarashi et al., 2012b; Matsunaga et al., 2013; Fujii et al., 2014; Takahashi et al., 2015; Imamura et
834 al., 2017a; Muto et al., 2019). The downward movement slowed down over the remaining 4 to 5
835 years. At the end of the observation period, about 85% of the total activity remains in the mineral soil,
836 including more than 10% below 5 cm depth. This average evolution, however, must not hide the
837 disparity observed among forest sites, especially in the first 2 to 3 years, which was ascribed to
838 differences in the canopy density or the thickness of the organic layer (e.g. Koarashi et al. 2012b,
839 2016a; Coppin et al., 2016; Shoko et al., 2017; Takahashi et al. 2018). Despite strongly variable
840 activity levels in deep layers, it seems that the relative partitioning between the three mineral horizons

841 had already taken shape in 2011, according to the following distribution: 85% in the 0-5 cm layer,
842 10% in the 5-10 cm layer and 5% below, and did not change until the end of the observation period. At
843 the few sites where soil profiles were finely sampled in depth, it was demonstrated that the activity
844 sharply decreased with depth according to a roughly exponential profile over the first 5-10
845 centimetres, which established quite rapidly and slowly diffused with years (Koarashi et al., 2012b;
846 Teramage et al., 2014b, 2016; Takahashi et al., 2015, 2018; Yoschenko et al., 2017; Muto et al. 2019).
847 The relaxation length (e.g. see definition in Kato et al., 2012b) already increased to 1-2.5cm in less
848 than a few months (Koarashi et al., 2012b; Teramage et al., 2014b; Takahashi et al., 2018) then very
849 slowly increased with years, e.g. by less than 0.5 cm in 6 years at the coniferous sites monitored by
850 KATO group (Takahashi et al., 2018). Muto et al. (2019) demonstrated that the spatio-temporal
851 evolution of activity profiles measured at KOARA sites could be reasonably predicted by a simple
852 diffusion equation, where the diffusion coefficient rapidly decreased with years (i.e. by nearly 2 orders
853 of magnitude in 4 years). It is worth noting that, to keep 85% of the activity inventory in the top 5
854 centimeters (as demonstrated above), we have to impose a relaxation length of 2.75cm. Assuming an
855 exponential profile with such a characteristic length, however, underestimates the proportion of the
856 activity contained in the deepest 10-20cm layer, as it predicts only ~1.5% against 5% in reality. As
857 already pointed out by the authors mentioned above, the mean activity profile does not follow an
858 exponential shape below 5-cm depth anymore, because of a deep (and early) penetration of a small
859 proportion of deposited radiocesium, due to processes that have still to be elucidated (e.g. preferential
860 flow paths through macro-porosities, colloidal transport, inhibition of absorption by soil organic
861 matter).

862 The best estimates of effective migration rates were estimated by taking into account the
863 uncertainties in soil densities, M_{SL} and ρ_j , as well as the sources of uncertainties influencing the
864 allocation factor α_{TE} (e.g. stand age, biomass increment, litterfall and K concentration ratio). The mean
865 ρ_j 's were estimated by averaging among sites and over time (at same site) the site-specific values
866 either measured or deduced from the inventory-to-concentration ratio. We derived the following
867 ranges of variation: $\rho_{S5}=370\pm 50$ kg d.w. m⁻³ ([245-535]), $\rho_{S10}=500\pm 65$ kg d.w. m⁻³ ([345-685]) and

868 $\rho_{s20}=520\pm55$ kg d.w. m^{-3} [375-695]. As explained in section 1.4.4, the best estimate was calculated for
869 any layer j by minimizing the sum of the MSLEs on predicted activity inventory and concentration in
870 that layer (see examples of calculated errors in Fig. S7c,d). The results are summarized in Table 2 for
871 varying f 's. Whatever f , the effective migration rate was easily identifiable for the top organic layer
872 because minima were well marked for both types of errors and pointed to approximately the same
873 number. We notice that errors in the activity inventory are much less dispersed than those attached to
874 the activity concentration because S_{SL} is not impacted mathematically by the variability of soil density.
875 The best-estimate λ_{SL} which slightly depends on the interception fraction amounts to about $1.3 \cdot 10^{-3} d^{-1}$,
876 in quite good agreement with the estimate given above based on the activity peak characteristics in
877 summer 2011. This corresponds to a mean residence time of about 1.5 year. It is shorter than the
878 characteristic time of organic matter decomposition generally measured in Japanese coniferous forests,
879 which typically varies in the range 2.5 ± 1.3 y ([0.5-5.0]) (e.g. Nakane et al., 1984, 1995; Ichikawa et
880 al., 2003b; Shutou and Nakane, 2004; Joo et al., 2006; Osono et al., 2007; Kurihara et al., 2018;
881 Toriyama et al., 2018). This is due to the percolation of contaminated rainfall and throughfall waters
882 through the organic layer according to kinetics faster than organic matter decomposition. The situation
883 for the underlying 0-5 cm mineral layer is less clear because minima in the RMSLEs are much less
884 pronounced and indicate different numbers depending on whether inventory or concentration is looked
885 at. However, the simulations suggest that the best-estimate rate that slightly depends on the
886 interception fraction would typically range between 2.2 and $3 \cdot 10^{-4} d^{-1}$, despite some imprecision (cf.
887 Table 2). This gives a mean residence time between 6.5 to 8.5 years, which is definitely longer than in
888 the above layer due to the immobilization/fixation of a large proportion of incoming radiocesium
889 through a variety of physico-chemical mechanisms. Such a residence times correspond to migration
890 velocities between 0.59 and 0.77 cm y^{-1} , in the lower range of those measured by Mishra et al. (2018)
891 in Fukushima coniferous forest soils based on a few measurements of activity profiles in 2012 and
892 2013. A simplified approach to estimate the residence time τ in a mineral horizon of depth h is to
893 express it in terms of an apparent distribution coefficient, KD (l/kg), based on the following
894 relationship: $\tau \approx Ln(2)/I \times \rho \times h \times KD$ where I ($L m^{-2} y^{-1}$) represents the effective annual water percolation

895 flux across the layer. In coniferous forests of the Fukushima region, the percolation flux through the
896 top mineral layer can be roughly estimated by subtracting rainfall interception (by the above ground
897 vegetation) and evaporation from the annual precipitation. Looking at the literature dealing with
898 climatology and forest hydrology in Japanese coniferous forests (e.g. Komatsu et al., 2007, 2008a,b,
899 2010, 2012; Tsuruta et al., 2016; Laceby et al., 2016; Sun et al., 2017), we evaluated it to about 1000 L
900 $\text{m}^{-2} \text{y}^{-1}$. Thus, adopting the above relationship leads to KD 's ranging between 500 and 670 $\text{L kg}^{-1} \text{d.w.}$
901 for the upper 5-cm mineral layer, which is significantly smaller than the values provided by Ishikawa
902 et al. (2008) for upland soils in Japan ($\text{GM}=3900 \text{ L kg}^{-1} \text{d.w.}$). Our estimates are closer to the value
903 reported in the IAEA technical report (2010) for sandy soils ($\text{GM}=530 \text{ L kg}^{-1} \text{d.w.}$) than organic soils
904 ($\text{GM}=270 \text{ L kg}^{-1} \text{d.w.}$). Our estimate is about twice that reported by Mishra et al. (2018) for the 0-20
905 cm mineral soil of a few Fukushima coniferous forests, i.e. typically less than 250 $\text{L kg}^{-1} \text{d.w.}$
906 Regarding the 5-10 cm soil layer, the simulations seem to indicate a migration rate typically comprised
907 between $1 \cdot 10^{-3}$ and $2 \cdot 10^{-3} \text{ d}^{-1}$, although we notice that the model error has considerably increased. This
908 rate is about 5-fold higher than that estimated in the 0-5 cm layer which means that radiocesium is
909 much more mobile here than in the above layer. This suggests that a large proportion of radiocesium
910 present in this layer might be in a rather mobile form (in colloidal forms?) and no longer retained by
911 sorption/fixation processes onto the solid matrix. Elucidating this issue would require further
912 experimental investigation.

913 The mean activity concentrations and inventories predicted with the best-estimated migration
914 rates are shown in Fig. 11, Fig. 12 and Fig. S6. In spite of its simplicity, the model quite well mimics
915 the observations in the two first layers, both in terms of activity levels and kinetics. The results are
916 rather insensitive to interception fraction apart from the activity levels predicted in the organic layer in
917 the first few weeks. The predictions are much less satisfactory in the deeper layers than above,
918 especially in the first year. The discrepancy is particularly obvious for the 10-20 cm layer where the
919 activity inventory is under-estimated by more than one order of magnitude. The predicted kinetics is
920 definitely too slow. The model could never reproduce the rapid initial increase (or penetration) of
921 radiocesium contamination in the deep layers, while maintaining acceptable results in the 2 top layers.

922 Because of the complexity of the lixiviation/retention processes occurring in the soil column, the
923 modelling approach based on a simple retention time concept proves to be inadequate. To improve the
924 realism of the approach, it would very likely be necessary to differentiate several pools of radiocesium
925 subject to different kinds of retention mechanisms (e.g. instantaneous reversible sorption/desorption,
926 immobilization/remobilization by biological components, slow irreversible fixation onto mineral
927 components, colloidal transport, etc.). Such refined approaches (mostly 2-pool approaches) have been
928 implemented in dynamic forest models and tested against measurements made in forests contaminated
929 by Chernobyl accident (e.g. Schell et al., 1996; Linkov, 1995; Linkov et al., 1997; Linkov and Schell,
930 1999; Avila et al., 1999; IAEA BIOMASS, 2002; Goor and Avila, 2003; Calmon et al., 2015; Thiry et
931 al., 2018, 2020). More recently, Ota et al. (2016) tested a 3-pool approach to predict radiocesium in a
932 Fukushima forest soil column but were faced to the lack of reliable data on KD and other retention
933 kinetic rates.

934 3. Conclusion

935 In this study, we conducted a meta-analysis of field studies conducted over the period March
936 2011 - March 2017 in Japanese cedar and cypress plantations contaminated by atmospheric
937 radiocesium (^{137}Cs) fallouts. The review encompasses 41 forest sites located in the Fukushima and
938 neighbouring prefectures, with a majority of mature cedar forests planted on andosols, and
939 contaminated at levels varying from about 10 kBq m^{-2} to more than $1\,000 \text{ kBq m}^{-2}$ to the north-west of
940 the nuclear site. Hundreds of spatio-temporal measurements of the activity levels in aerial tree organs
941 and soil layers as well as measurements of the activity transfer by tree depuration were collected,
942 processed then analysed.

943 To enable comparison and reduce variability between sites, all radiological measurements were,
944 among other treatments, normalized by the deposit and interpolated onto the same spatio-temporal
945 frame (i.e. time frequency, vertical discretization of soil). It was demonstrated that normalization
946 strongly reinforced the consistency between site-specific observations, although some poorly
947 understood residual variability persisted which likely resulted from differences in the interception

948 fraction, forest stand and climate characteristics, measurement errors and uncertainties in the deposit
949 estimate. As this residual noise remained moderate with respect to the mean trend, we derived a
950 generic evolution of radiocesium in forest over the 6-yr period, by averaging observations over sites
951 (GM) and quantifying the residual dispersion (GSD). This mean dynamics was then discussed and
952 analysed with the help of a simple dynamic model involving few transfer processes (i.e. interception,
953 depuration, root uptake, foliar transfer, tree biomass growth, downward migration and physical decay)
954 and relying on empirical parametrizations (e.g. kinetic rates, mean residence times). The contribution
955 of each process and unknown transfer parameters were inferred by calibrating the model against time
956 observations, while varying the unknown interception ratio between 0.7 and 0.85 (most plausible
957 range).

958 In this study, we demonstrated that the activity levels and dynamics observed in the forest
959 compartments were consistent together and generally well reproduced by our simple mass balance
960 approach whatever the value of interception fraction (in the range imposed). For an interception ratio
961 of 0.85, we estimated that, on average, up to nearly 80% of the total deposit was transferred to the
962 forest floor due to depuration over the 6-year period, throughfall, litterfall and stemflow contributing
963 to respectively ~56%, ~22% and 1%. The mass balance analysis indicated that contribution of root
964 uptake to the contamination of tree vegetation (i.e. activity inventory) might have varied between 0%
965 and 5% of the total deposit after 6 years (depending on the interception ratio). The activity
966 concentrations in canopy organs (foliage, branches) rapidly decreased in the first few months then
967 more slowly after 2011, according to effective half-lives (1.4 years and 1.8 years, respectively) which
968 were much shorter than in stem bark (11.5 years). The mass balance analysis suggested that, whatever
969 interception fraction was, depuration processes participated to about 95% of the net decrease of
970 activity concentration in canopy organs, the remaining 5% being attributed to incorporation (2%),
971 physical decay (2%) and biological dilution (1%). The simulations further indicated that incorporation
972 might have contributed between 40% and 100% to the total activity transferred to stem wood after 6
973 years (depending on the interception fraction), the remaining part being induced by root uptake.

974 Regarding soil, our analysis demonstrated that activity levels in the upper organic layer peaked
975 in summer 2011 then decreased according to an effective half-life of 2.2 years. The mean residence
976 time of radiocesium in this layer was estimated to about 1.5 years, this value being, as expected,
977 significantly shorter than organic matter decomposition because of the percolation of rainfall and
978 throughfall waters. The characteristic times of the system are such that 50% of the activity inventory
979 in the forest floor had already moved in the mineral soil after 2 years and about 85% after 6 years.
980 Downward migration of radiocesium induced an initially rapid increase of contamination levels in all
981 mineral soils, due to likely the infiltration of some amount of initially exchangeable (mobile)
982 radiocesium after deposition. After summer 2011, the contamination levels continued to increase more
983 slowly in all mineral layers, while the partitioning of radiocesium inventory between horizons
984 remained remarkably constant until the end of the observation period: 85% in the 0-5 cm layer, 10% in
985 the 5-10 cm layer and 5% in the 10-20 cm layer. In the top 5 cm mineral layer, the mean residence
986 time amounted to approximately 7.5 years, due to its high capacity to immobilize radiocesium
987 incoming from the above organic layer through a variety of physico-chemical mechanisms already
988 discussed in the literature. Finally, our compartmental approach based on retention times proved to be
989 inadequate and could not mimic the dynamics observed in the mineral soil layers below 5 cm depth,
990 due to likely the complexity of lixiviation/retention processes in the soil column.

991 Beyond these results, the database constituted in this study will undoubtedly help improving the
992 process-based dynamic models developed after the Chernobyl accident or currently being tested
993 against Fukushima observations (e.g. Schell et al., 1996; Avila et al., 1999; Linkov and Schell, 1999;
994 Shaw et al., 2005; IAEA BIOMASS, 2002; Goor and Avila, 2003; Hashimoto et al., 2013; Calmon et
995 al., 2015; Nishina et al., 2015, 2018; Ota et al., 2016; Diener et al., 2017; Thiry et al. 2018, 2020).

996 **Supporting Information**

997 Supporting Information includes six sections: (section S.1) the description of forest site characteristics
998 considered in the review, (section S.2) the approach used for quantifying the growth of tree biomass in
999 Japanese cedar & cypress forests, (section S.3) supplementary data on radiocesium activity at specific

1000 sites, (section S.4) data on biomass litterfall, (sections S.5) data on activity inventory in soil layers and
1001 (section S.6) quantification of model errors.

1002 **Acknowledgement**

1003 This research was achieved thanks to the financial support by: (1) the French State financial support
1004 managed by the Agence Nationale de la Recherche, allocated in the “Investissements d’Avenir”
1005 framework program under reference ANR-11-RSNR-0002 and (2) Euratom research and training
1006 program 2014-2018 under grant agreement No 662287 for the TERRITORIES project, which was part
1007 of the EJP CONCERT.

1008 This publication reflects only the author's view. Responsibility for the information and views
1009 expressed therein lies entirely with the authors.

1010 **References**

1011 Avila, R., Moberg, L., Hubbard, L., Fesenko, S., Spiridonov, S., Alexakhin, R. (1999)
1012 Conceptual Overview of Forestland - A Model to Interpret and Predict Temporal and Spatial Patterns
1013 of Radioactively Contaminated Forest Landscapes. NATO Science Series Vol. 58, 173-183.

1014 Boone, F.W., Kantelo, M.V., Mayer, P.G., Palms, J.M., (1985) Residence half-times of ^{129}I in
1015 undisturbed surface soils based on measured soil concentration profiles. Health Physics, 48: 401–413.

1016 Bunzl K., Schimmack W., Kreutzer K. and Schierl R., (1989) Interception and retention of
1017 Chernobyl-derived ^{134}Cs , ^{137}Cs and ^{106}Ru in a spruce stand. Science of the Total Environment, 78:
1018 77-87.

1019 Calmon P., Gonze M.-A. and Murlon C. (2015) Early-phase Redistribution of
1020 RadioCesiumFallouts in an Evergreen Coniferous Forest after Chernobyl and Fukushima Accidents.
1021 Science of Total Environment, 529: 30-39

- 1022 Casadesus J., Sauras-Yera T., Vallejo V.R. (2008) Predicting soil-to-plant transfer of
1023 radionuclides with a mechanistic model (BioRUR). *Journal of Environmental Radioactivity*, 99:864-
1024 71
- 1025 Coppin F., Hurtevent P., Loffredo N., Simonucci C., Julien A., Gonze M.A., Nanba K., Onda Y.
1026 and Thiry Y. (2016) Radiocesium Partitioning in Japanese Cedar Forests Following the Early Phase
1027 of Fukushima fallout Redistribution. *Scientific Reports*, 6, 37618.
- 1028 Diener A., Diener, Hartmann P., Urso L., Vives i Batlle J., Gonze M.A., Calmon P., Steiner M.,
1029 (2017) Approaches to modelling radioactive contaminations in forests - Overview and guidance.
1030 *Journal of Environmental Radioactivity*, 178-179 :203-211
- 1031 Endo I., Ohte N., Iseda K., Tanoi K., Hirose A., Kobayashi N.I., Murakami M., Tokuchi N.,
1032 Ohashi M. (2015) Estimation of radioactive ¹³⁷-cesium transportation by litterfall, stemflow and
1033 throughfall in the forests of Fukushima. *Journal of Environmental Radioactivity*, 149, 176-185.
- 1034 Fesenko SV, Soukhova NV, Sanzharova NI, Avila R, Spiridonov SI, Klein D, Badot P-M,
1035 (2001) ¹³⁷Cs availability for soil to understory transfer in different types of forest ecosystems. *Sci*
1036 *Total Environ*, 269:87–103
- 1037 Frissel M.J. and Pennders R. (1983) Models for the accumulation and migration of ⁹⁰Sr, ¹³⁷Cs,
1038 ^{239,240}Pu, ²⁴¹Am in the upper layer of soils. In: Coughtrey, P.J., Bell, J.N.B., Roberts, T.M. (Eds.),
1039 *Ecological Aspects of Radionuclide Release*. Blackwell, Oxford, pp. 63–72.
- 1040 Fujii K., Ikeda S., Akama A., Komatsu M., Takahashi M. & Kaneko S. (2014) Vertical
1041 migration of radiocesium and clay mineral composition in five forest soils contaminated by the
1042 Fukushima nuclear accident. *Soil Science and Plant Nutrition*, 60:6, 751-764
- 1043 Fujii, K., Yamaguchi, N., Imamura, N., Kobayashi, M., Kaneko, S., Takahashi, M., (2019)
1044 Effects of radiocesium fixation potentials on ¹³⁷Cs retention in volcanic soil profiles of Fukushima
1045 forests. *J. Environ. Radioact.* 198: 126–134.
- 1046 Fukuda, M., Iehara, T. & Matsumoto, M. (2003) Carbon stock estimates for sugi and hinoki
1047 forests in japan. *Forest Ecology and Management*, 184(1-3):1–16.

- 1048 Gonze M.A., Renaud P., Korsakissok I., Kato H., Hinton T.G., Mourlon C. and Simon-Cornu
1049 M. (2014) Assessment of Dry and Wet Atmospheric Deposits of Radioactive Aerosols: Application to
1050 Fukushima RadioCesiumFallout. *Environ. Sci. Technol.*, 48: 11268–11276.
- 1051 Gonze M.-A., Mourlon C., Calmon P., Manach E., Debayle C., Baccou J. (2015) Modeling the
1052 Dynamics of Ambient Dose Rates Induced by RadioCesium in the Fukushima Terrestrial Environment.
1053 *Journal of Environmental Radioactivity*, 215: 1–13
- 1054 Gonze M.-A. & Calmon P., (2017) Meta-analysis of radiocesium contamination data in Japanese
1055 forest trees over the period 2011-2013. *Sci. Total Environ.*, 601–602 : 301–316.
- 1056 Goor F. and Avila R. (2003) Quantitative comparison of models of ¹³⁷Cs cycling in forest
1057 ecosystems. *Environmental Modelling & Software*, 18: 273–279.
- 1058 Goor F and Thiry Y (2004) Processes, dynamics and modelling of radioCesium cycling in a
1059 chronosequence of Chernobyl-contaminated Scots pine (*Pinus sylvestris* L.) plantations. *Sci Total*
1060 *Environ*, 325:163–180
- 1061 Haibara, K. & Aiba, Y. (1982) Nutrient content of throughfall in a sugi (*cryptomeria japonica*)
1062 stand soon after crown closure. *Bulletin of the Experiment Forests – Tokyo University of Agriculture*
1063 *and Technology (Japan)*.
- 1064 Hara, T., Takenaka, C., Tomioka, R. (2020) Change in the chemical form of ¹³⁷Cs with age in
1065 needles of Japanese cedar. *Journal of Environmental Radioactivity*, 213, 106137.
- 1066 Hashimoto S., Ugawa S., Nanko K., Shichi K. (2012) The total amounts of radioactively
1067 contaminated materials in forests in Fukushima, Japan, *Scientific Reports*, 2: 416
- 1068 Hashimoto, S., Matsuura, T., Nanko, K., Linkov, I., Shaw, G., Kaneko, S., (2013) Predicted
1069 spatio-temporal dynamics of radiocesium deposited onto forests following the Fukushima nuclear
1070 accident. *Sci. Rep.*, 3: 2564.
- 1071 Hiruta T., Kawaguchi C., Suda T., Tsuboyama Y., Otani Y., Kobayashi M., Shinomiya Y.,
1072 (2016) Radiocesium dynamics in the litter fall and forest floor. *Tohoku J. For. Sci.* 21(2):43–49.

1073 Hisadome K., Onda Y., Kawamori A., Kato H. (2013) Migration of radioCesiumwith litterfall
1074 in hardwood-Japanese red pine mixed forrst and Sugi plantation. J. Jpn. For. Soc., 95: 267-274.

1075 Hurtevent P. et al. (in prep.) Five-year monitoring (2013-2018) and analysis of ^{137}Cs , ^{133}Cs
1076 and K recycling in 2 Japanese cedar forest of the Fukushima region.

1077 IAEA (2002) Modelling the migration and accumulation of radionuclides in forest ecosystems.
1078 Report of the Forest Working Group of the Biosphere Modelling and Assessment (BIOMASS)
1079 Programme, Theme 3. International Atomic Energy Agency, Vienna.

1080 IAEA (2010) Handbook of parameter values for the prediction of radionuclide transfer
1081 interrestrial and freshwater environments. In: Technical Report Series TR472. International Atomic
1082 Energy Agency, Vienna STI/PUB/472; ISBN 92-0-113009-9.

1083 Ichikawa, T., Takahashi, T. & Asano, Y. (2003a) Effects of the conversion of forest
1084 management type from natural deciduous broadleaved forests to artificial Japanese cypress
1085 (*Chamaecyparis obtusa*) and Japanese cedar (*Cryptomeria japonica*) forests on nutrient dynamics.
1086 *Jpn.J.For.Environment*, 45:35-42.

1087 Ichikawa T., Yamaguchi T., Takahashi T. & Asano Y., (2003b) Effects of the conversion of the
1088 forest management type from natural deciduous broadleaved forests to artificial Japanese cypress
1089 (*Chamaecyparis obtusa*) and Japanese cedar (*Cryptomeria japonica*) forests on soil microbial flora and
1090 mineralization characteristics of organic carbon. *Jpn. J. For. Environ* 45, 81-87.

1091 Iizuka K., Toya N., Ohshima J., Ishiguri F., Miyamoto N., Aizawa M., Ohkubo T., Takenaka C.
1092 & Yokota S. (2018) Relationship between ^{137}Cs concentration and potassium content in stem wood
1093 of Japanese cedar (*Cryptomeria japonica*). *Journal of Wood Science*, 64:59-64

1094 Imamura, N., Komatsu, M., Ohashi, S., Hashimoto, S., Kajimoto, T., Kaneko, S., Takano, T.,
1095 (2017a) Temporal changes in the radiocesium distribution in forests over the five years after the
1096 Fukushima Daiichi Nuclear Power Plant accident. *Sci. Rep.*, 7: 8179

- 1097 Imamura N., Levia D.F., Toriyama J., Kobayashi M., Nanko K. (2017b) Stemflow-induced
1098 spatial heterogeneity of radiocesium concentrations and stocks in the soil of a broadleaved deciduous
1099 forest. *Science of the Total Environment*, 599–600 : 1013–1021
- 1100 Inagaki Y., Kuramoto S. & Fukata H. (2010a) Effects of typhoons on leaf fall in hinoki cypress
1101 (*Chamaecyparis obtusa* Endlicher) plantations in Shikoku Island. *Bulletin of FFPRI*, Vol.9 No.3
1102 (No.416) 103 - 112.
- 1103 Inagaki Y., Okuda S., Sakai A., Nakanishi A., Shibata S., Fukata H. (2010b. Leaf-litter
1104 nitrogen concentration in hinoki cypress forests in relation to the time of leaf fall under different
1105 climatic conditions in Japan. *Ecol Res*, 25: 429–438
- 1106 Inagaki Y., Inagaki M., Hashimoto T., Kobayashi M., Itoh Y., Shinomiya Y., Fujii K., Kaneko
1107 S. & Yoshinaga S. (2012) Aboveground production and nitrogen utilization in nitrogen-saturated
1108 coniferous plantation forests on the periphery of the kanto plain. *Bulletin of FFPRI*, Vol.11 No.3
1109 (No.424) 161 – 173.
- 1110 Ishikawa, N.K., Uchida, S., Tagami, K., (2008) Distribution coefficients for ⁸⁵Sr and ¹³⁷Cs in
1111 Japanese agricultural soils and their correlation with soil properties. *J. Radioanal. Nucl. Chem.*,
1112 277:433–439.
- 1113 Itoh Y., Imai A., Kobayashi M. (2015) Initial radiocesium deposition on forest ecosystems
1114 surrounding the Tokyo metropolitan area due to the Fukushima Daiichi Nuclear Power Plant accident.
1115 *Hydrological Research Letters*, 9(1): 1-7.
- 1116 Japanese Forestry Agency, (2019) Annual report on forest and forestry in Japan (Fiscal Year
1117 2018).
- 1118 Joo S.J., Yim M.H., Nakane K. (2006) Contribution of microarthropods to the decomposition of
1119 needle litter in a Japanese cedar (*Cryptomeria japonica* D. Don) plantation. *For. Ecol. Manag.*,
1120 234:192–198.
- 1121 Kajimoto T., Saito S., Kawasaki T., Kabeya D., Yazaki K., Tanaka H., Ota T., Matsumoto Y.,
1122 Tabuchi R., Kiyono Y., Takano T., Kuroda K., Fujiwara T., Suzuki Y ;, Komatsu M., Ohashi S.,

1123 Kaneko S., Akama A., Takahashi M. (2015) Dynamics of radiocesium in forest ecosystems affected
1124 by the Fukushima Daiichi Nuclear Power Plant accident: species-related transfer processes of
1125 radiocesium from tree crowns to ground floor during the first two years. *J. Jpn. For. Soc.*, 97: 33-43.

1126 Kanasashi T., Sugiura Y., Takenaka C., Hijii N., Umemura M. (2015) Radiocesium distribution
1127 in sugi (*Cryptomeria japonica*) in Eastern Japan: translocation from needles to pollen. *Journal of*
1128 *Environmental Radioactivity*, 139: 398-406.

1129 Kanasashi T., Takenaka C., Sugiura Y., Hijii N., Umemura M. (2016) Inferring the chemical
1130 form of ¹³⁷Cs deposited by the Fukushima Dai-ichi Nuclear Power Plant accident by measuring
1131 ¹³⁷Cs incorporated into needle leaves and male cones of Japanese cedar trees. *Science of Total*
1132 *Environment*, 553: 643-649.

1133 Kaneko, N., Katagiri, S., Yamashita, H. & Kitaoka, N. (1997) A long term observation of
1134 litterfall of japanese red cedar [*Cryptomeria japonica*] in Sanbe experimental forest of Shimane
1135 university [Japan]. *Bulletin of the Faculty of Life and Environmental Science - Shimane University*
1136 (Japan).

1137 Kaneko S, Ikeda S, Akama A, Miura S, Takahashi M (2013) Soil physicochemical properties of
1138 experimental sites in forests contaminated by radioactive materials due to the Fukushima Daiichi
1139 Nuclear Power Plant accident. *Jpn. J. For. Environ.*, 55:75–81.

1140 Kang S., Yoneda M., Shimada Y., Satta N., Fujita Y. & Shin I. H.. (2017) Interpreting the
1141 deposition and vertical migration characteristics of ¹³⁷Cs in forest soil after the Fukushima Dai-ichi
1142 Nuclear Power Plant accident. *Environ Monit Assess*, 189: 384

1143 Karadeniz Ö, Karakurt H, Çakır R, Çoban F, Büyükok E, Akal C, (2015) Persistence of ¹³⁷Cs
1144 in the litter layers of forest soil horizons of Mount İDA/Kazdagi, Turkey. *J Environ Radioact.*,
1145 139:125–134

1146 Katagiri S., Kaneko. N., Obatake. Y. (1990) Nutrient cycling in a sugi (*cryptomeria japonica* D.
1147 Don) stand with insufficient management: nutrient accumulation in aboveground and soil and nutrient
1148 return by litterfall and rainfall. *Bull Fac Agr, Shimane Univ*, 24:21–27.

- 1149 Kato H., Onda Y., Gomi T. (2012a) Interception of the Fukushima reactor accident-derived
1150 ^{137}Cs , ^{134}Cs and ^{131}I by coniferous forest canopies. *Geophysical Research Letters*, vol. 39, L20403.
- 1151 Kato, H., Onda, Y., Teramaga, M., (2012b) Depth distribution of ^{137}Cs , ^{134}Cs and ^{131}I in soil
1152 profile after Fukushima Dai-ichi Nuclear power plant accident. *J. Environ. Radioact.*, 111: 59-64.
- 1153 Kato H. and Onda Y. (2014) Temporal changes in the transfer of accidentally released ^{137}Cs
1154 from tree crowns to the forest floor after the Fukushima Daiichi Nuclear Power Plant accident.
1155 *Progress in Nuclear Science and Technology*, 4:18-22.
- 1156 Kato H., Onda Y., Hisadome K., Loffredo N., Kawamori A. (2017) Temporal changes in
1157 radiocesium deposition in various forest stands following the Fukushima Dai-ichi Nuclear Power Plant
1158 accident. *Journal of Environmental Radioactivity*, 166: 449-457.
- 1159 Kato, H., Onda, Y., Wakahara, T., Kawamori, A., (2018) Spatial pattern of atmospherically
1160 deposited radiocesium on the forest floor in the early phase of the Fukushima Daiichi Nuclear Power
1161 Plant accident. *Sc. Tot. Environ.*, 615: 187-196
- 1162 Kato, H. and Onda, Y., (2018) Determining the initial Fukushima reactor accident-derived
1163 cesium-137 fallout in forested areas of municipalities in Fukushima Prefecture. *J. For. Res.* 23, 73–84.
- 1164 Kato H., Onda Y., Saidin Z.H., Sakashita W., Hisadome K., Loffredo N., (2019) Six-year
1165 monitoring study of radiocesium transfer in forest environments following the Fukushima nuclear
1166 power plant accident. *Journal of Environmental Radioactivity*, 210:105817
- 1167 Katsuno, M, Hagihara, A, Hozumi, K (1984) Litterfall of a Japanese cedar (*Cryptomeria*
1168 *japonica*) stand. *Jpn. For. Soc.*, 363–364.
- 1169 Koarashi, J., Moriya, K., Atarashi-Andoh, M., Matsunaga, T., Fujita, H., Nagaoka, M. (2012a)
1170 Retention of potentially mobile radiocesium in forest surface soils affected by the Fukushima nuclear
1171 accident. *Scientific Reports*, 1:1005.

- 1172 Koarashi, J., Atarashi-Andoh, M., Matsunaga, T., Sato, T., Nagao, S., Nagai, H., (2012b)
1173 Factors affecting vertical distribution of Fukushima accident-derived radiocesium in soil under
1174 different land-use conditions. *Sci. Total Environ.*, 431 : 392–401.
- 1175 Koarashi, J., Atarashi-Andoh, M., Takeuchi, E., Nishimura, S., (2014) Topographic
1176 heterogeneity effect on the accumulation of Fukushima-derived radiocesium on forest floor driven by
1177 biologically mediated processes. *Sci. Rep.*, 4: 6853.
- 1178 Koarashi, J., Atarashi-Andoh, M., Matsunaga, T., Sanada, Y., (2016a) Forest type effects on the
1179 retention of radiocesium in organic layers of forest ecosystems affected by the Fukushima nuclear
1180 accident. *Sci. Rep.*, 6: 38591.
- 1181 Koarashi, J., Nishimura, S., Nakanishi, T., Atarashi-Andoh, M., Takeuchi, E., Muto, K.,
1182 (2016b) Post-deposition early-phase migration and retention behaviour of radiocesium in a litter -
1183 mineral soil system in a Japanese deciduous forest affected by the Fukushima nuclear accident.
1184 *Chemosphere*, 165: 335–341.
- 1185 Koarashi, J., Atarashi-Andoh, M., (2019) Low ¹³⁷Cs retention capability of organic layers in
1186 Japanese forest ecosystems affected by the Fukushima nuclear accident. *J. Radioanal. Nucl. Chem.*,
1187 320: 179–191.
- 1188 Kobayashi, R., Kobayashi, N., Tanoi, K., Masumori, M., Tange, T., (2019) Potassium supply
1189 reduces cesium uptake in Konara oak not by an alteration of uptake mechanism, but by the uptake
1190 competition between the ions. *J. Environ. Radioac.*, 208-209: 106032
- 1191 Koizumi A., Niisoe T., Harada K.H., Fujii Y., Adachi A., Hitomi T., Ishikawa H. (2013) ¹³⁷Cs
1192 trapped by biomass within 20 km of the Fukushima Daiichi Nuclear Power Plant. *Environmental*
1193 *Science and Technology*, 47, 9612-9618.
- 1194 Komatsu, H., Tanaka, N., Kume, T., (2007) Do coniferous forests evaporate more water than
1195 broad-leaved forests in Japan? *J. Hydrol.*, 336:361–375.

- 1196 Komatsu, H., Kume, T., Otsuki, K., (2008a) The effect of converting a native broadleaved forest
1197 to a coniferous plantation forest on annual water yield: a paired catchment study in northern Japan.
1198 *Forest Ecol. Manage.*, 255: 880–886.
- 1199 Komatsu, H., Maita, E., Otsuki, K., (2008b) A model to estimate annual forest
1200 evapotranspiration in Japan from mean annual temperature. *J. Hydrol.*, 348:330–340.
- 1201 Komatsu, H., Kume, T., Otsuki, K., (2010) A simple model to estimate monthly forest
1202 evapotranspiration in Japan from monthly temperature. *Hydrol. Process.*, 24: 1896–1911.
- 1203 Komatsu H., Cho J., Matsumoto K., Otsuki K. (2012) Simple modeling of the global variation
1204 in annual forest evapotranspiration. *Journal of Hydrology*, (420-421): 380-390
- 1205 Komatsu M., Kaneko S., Ohashi S., Kuroda K., Sano T., Ikeda S., Saito S., Kiyono Y.,
1206 Tonosaki M., Miura S., Akama A., Kajimoto T., Takahashi M. (2016) Characteristics of initial
1207 deposition and behavior of radiocesium in forest ecosystems of different locations and species affected
1208 by the Fukushima Daiichi Nuclear Power Plant accident. *Journal of Environmental Radioactivity*, 161:
1209 2-10.
- 1210 Konopleva I, Klemm E, Konoplev A, Zibold G, (2009) Migration and bioavailability of ¹³⁷Cs in
1211 forest soil of southern Germany. *J Environ Radioact*, 100:315–321
- 1212 Koya P.R., Goshu A.T. (2013) Solutions of Rate-state Equation Describing Biological
1213 Growths. *American Journal of Mathematics and Statistics* 2013, 3(6): 305-311
- 1214 Kruyts N, Delvaux B, (2002) Soil organic horizons as a major source for radiocesium
1215 biorecycling in forest ecosystems. *J EnvironRadioact*, 52:175–190
- 1216 Kurihara M., Onda Y., Kato H., Loffredo N., Yasutaka T., Coppin F. (2018) Radiocesium
1217 migration in the litter layer of different forest types in Fukushima, Japan. *Journal of Environmental*
1218 *Radioactivity*, 187: 81-89.

- 1219 Kuroda K., Kagawa A., Tonosaki M. (2013) Radiocesium concentrations in the bark, sapwood
1220 and heartwood of three species collected at Fukushima forests half a year after the Fukushima Dai-ichi
1221 nuclear accident. *Journal of Environmental Radioactivity*, 122, 37-42.
- 1222 Laceby J.P., Chartin C., Evrard O., Onda Y., Garcia-Sanchez L. & Cerdan O. (2016) Rainfall
1223 erosivity in catchments contaminated with fallout from the Fukushima Daiichi nuclear power plant
1224 accident. *Hydrol. Earth Syst. Sci.*, 20:2467–2482.
- 1225 Linkov I. (1995) Radionuclide Transport in Forest Ecosystems: Modelling Approaches and
1226 Safety Evaluation. PhD Thesis, University of Pittsburgh, 171 p.
- 1227 Linkov I., Morel B. & Schell W. R. (1997) Remedial policies in radiologically contaminated
1228 forests: environmental consequences and risk assessment. *Risk Analysis* 17, 67–75.
- 1229 Linkov, I. and Schell, W.R. (Eds.), (1999) Contaminated Forests: Recent Developments in
1230 Risk Identification and Future Perspectives. Kluwer Academic Publishers.
- 1231 Loffredo N., Onda Y., Kawamori A., Kato H. (2014) Modeling of leachable ¹³⁷Cs in
1232 throughfall and stemflow for Japanese forest canopies after Fukushima Daiichi Nuclear Power Plant
1233 accident. *Science of the Total Environment*, 493, 701-707.
- 1234 Loffredo N., Onda Y., Hurtevent P., Coppin F. (2015) Equation to predict the ¹³⁷Cs leaching
1235 dynamic from evergreen canopies after a radio-caesium deposit. *Journal of Environmental*
1236 *Radioactivity*, 147, 100-107.
- 1237 MAFF (2011) Ministry of Agriculture Forestry and Fisheries of Japan Annual report on forest
1238 and Forestry in Japan (Fiscal year 2011). [http://www.maff.go.jp/e/data/publish/attach/pdf/index-](http://www.maff.go.jp/e/data/publish/attach/pdf/index-27.pdf)
1239 [27.pdf](http://www.maff.go.jp/e/data/publish/attach/pdf/index-27.pdf).
- 1240 MAFF (2012) The Results of Investigation on Radionuclides Distribution in Forest
1241 Environment in 2011. <http://www.rinya.maff.go.jp/j/press/kenho/pdf/130329-01.pdf>
- 1242 Mahara Y, Ohta T., Ogawa H. & Kumata A. (2014) Atmospheric Direct Uptake and Long-term
1243 Fate of Radiocesium in Trees after the Fukushima Nuclear Accident. *Scientific Reports*, 4:7121

- 1244 Manaka T., Imamura N., Kaneko S., Miura S., Furusawa H., Kanasashi T. (2019) Six-year
1245 trends in exchangeable radiocesium in Fukushima forest soils. *Journal of Environmental Radioactivity*
1246 203 : 84–92
- 1247 Masumori, M., Nogawa, N., Sugiura, S., Tange, T., (2015) Radiocesium in stem, branch and
1248 leaf of *Cryptomeria japonica* and *Pinus densiflora* trees: cases of forests in Minamisoma in 2012 and
1249 2013. *J. Jpn. For. Soc.*, 97: 51-56.
- 1250 Matsunaga, T., Koarashi, J., Atarashi-Andoh, M., Nagao, S., Sato, T., Nagai, H., (2013)
1251 Comparison of the vertical distributions of Fukushima nuclear accident radiocesium in soil before and
1252 after the first rainy season, with physicochemical and mineralogical interpretations. *Sci. Total*
1253 *Environ.*, 447: 301–314.
- 1254 Mishra S., Sahoo S.K., Bossew P., Sorimachi A., Tokonami S., (2018) Reprint of “Vertical
1255 migration of radio-Cesium derived from the Fukushima Dai-ichi Nuclear Power Plant accident in
1256 undisturbed soils of grassland and Forest”. *Journal of Geochemical Exploration*, 184: 271–295
- 1257 Miura, S. (2000) Proposal for a new definition to evaluate the status of forest floor cover and
1258 floor cover percentage (fcp) from the viewpoint of the protection against raindrop splash. *Journal of*
1259 *the Japanese Forestry Society*, 82(2):132–140.
- 1260 Miyamoto K., Okuda S., Inagaki Y., Noguchi M., Itou T. (2013) Within- and between-site
1261 variations in leaf longevity in hinoki cypress (*Chamaecyparis obtusa*) plantations in southwestern
1262 Japan. *J For Res*, 18:256–269
- 1263 Murakami, M., Ohte, N., Suzuki, T., Ishii, N., Igarashi, Y., Tanoi, K., (2014) Biological
1264 proliferation of cesium-137 through the detrital food chain in a forest ecosystem in Japan. *Sci. Rep.*,
1265 4:3599.
- 1266 Muto K., Atarashi-Andoh M., Matsunaga T., Koarashi J., (2019) Characterizing vertical
1267 migration of ¹³⁷Cs in organic layer and mineral soil in Japanese forests: Four-year observation and
1268 model analysis. *Journal of Environmental Radioactivity*, 208–209 : 106040

- 1269 Myttenaere, C., Schell, W.R., Thiry, Y., Sombre, L., Ronneau, C., van der Stegen de Schrieck,
1270 J., (1993) Modelling of Cs-137 cycling in forests: developments and research needed. *Sci. Total*
1271 *Environ.* 136, 77-91.
- 1272 Nagakura J., Abe H., Zhang C., Takano T., Takahashi M., (2017) Cesium, rubidium and
1273 potassium content in the needles and wood of Japanese cedar trees harvested from the sites of different
1274 radiocesium deposition levels. *Jpn. J. For. Environ* 58, 51-59.
- 1275 Nakane K., Tsubota H. & Yamamoto M. (1984) Cycling of soil carbon in a Japanese red pine
1276 forest. I. Before a clear-felling. *Botanical Magazine, Tokyo* 97: 39–60.
- 1277 Nakane, K. (1995) Soil carbon cycling in a japanese cedar (*cryptomeria japonica*) plantation.
1278 *Forest Ecology and Management*, 72(2):185 – 197.
- 1279 Nakanishi T, Matsunaga T, Koarashi J, Atarashi-Andoh M, (2014) 137Cs vertical migration in a
1280 deciduous forest soil following the Fukushima Dai-ichi Nuclear Power Plant accident. *J Environ*
1281 *Radioact* 128:9–14.
- 1282 Niizato T., Abe H., Mitachi K., Sasaki Y., Ishii Y., Watanabe. T. (2016) Input and output
1283 budgets of radiocesium concerning the forest floor in the mountain forest of Fukushima released from
1284 the TEPCO's Fukushima Dai-ichi nuclear power plant accident. *Journal of Environmental*
1285 *Radioactivity*, 161: 11-21
- 1286 Nishikiori T., Watanabe M., Koshikawa M.K., Takamatsu T., Ishii Y., Ito S., Takenaka A.,
1287 Watanabe K., Hayashi S. (2015) Uptake and translocation of radiocesium in cedar leaves following
1288 the Fukushima nuclear accident. *Science of the Total Environment*, 502, 611-616.
- 1289 Nishikiori, T., Watanabe, M., Koshikawa, M., Watanabe, K., Yamamura, S., Hayashi, S.,
1290 (2019) 137Cs transfer from canopies onto forest floors at Mount Tsukuba in the four years following
1291 the Fukushima nuclear accident. *Sc. Tot. Environ.* 659, 783-789
- 1292 Nishina, K. and Hayashi, S., (2015) Modeling radionuclide Cs and C dynamics in an artificial
1293 forest ecosystem in Japan FoRothCs ver1.0. *Front. Environ. Sci.*, 3:61.

- 1294 Nishina K., Hashimoto S., Imamura N., Ohashi S., Komatsu M., Kaneko S., Hayashi S. (2018)
1295 Calibration of forest ^{137}Cs cycling model "FoRothC" via approximate Bayesian computation based
1296 on 6-year observations from plantation forests in Fukushima. *Journal of Environmental Radioactivity*,
1297 193–194:82–90
- 1298 NRA (2017) Nuclear Regulatory Authority Monitoring information of environmental
1299 radioactivity level. Available on <http://radioactivity.nsr.go.jp/en/>.
- 1300 Ohashi, S., Okada, N., Tanaka, A., Nakai, W., Takano, S., (2014) Radial and vertical
1301 distributions of radiocesium in tree stems of *Pinus densiflora* and *Quercus serrata* 1.5 y after the
1302 Fukushima nuclear disaster. *J. Environ. Radioact.* 134 : 54–60.
- 1303 Ohashi S., Kuroda K., Takano T., Suzuki Y., Fujiwara T., Abe H., Kagawa A., Sugiyama M.,
1304 Kubojima Y., Zhang C., Yamamoto K. (2017) Temporal trends in ^{137}Cs concentrations in the bark,
1305 sapwood, heartwood, and whole wood of four tree species in Japanese forests from 2011 to 2016.
1306 *Journal of Environmental Radioactivity*, 178-179: 335-342
- 1307 Ohno, T., Muramatsu, Y., Miura, Y., Oda, K., Inagawa, N., Ogawa, H., Yamazaki, A., Toyama,
1308 C., Sato, M., (2012) Depth profiles of radioactive cesium and iodine released from the Fukushima
1309 Daiichi nuclear power plant in different agricultural fields and forests. *Geochem. J.*, 46:287–295.
- 1310 Ohnui, K. and Mitchell, M.J., (1996) Elemental dynamics in a Japanese watershed with Sugi
1311 (*Cryptomeria japonica*) and Hinoki (*Chamaecyparis obtusa*) plantations. *Canadian Journal of Forest*
1312 *Research* 26, 2160-2169
- 1313 Okada N., Nakai W., Ohashi S., Tanaka A. (2015) Radiocesium migration from the canopy to
1314 the forest floor in pine and deciduous forests. *J. Jpn. For. Soc.*, 97: 57-62.
- 1315 Osono T., (2007) Decomposition processes of leaf litter and fungal communities in a cool
1316 temperate forest. *Jnp. J. Ecol.*, 57:304–318.
- 1317 Ota, M., Nagai, H., Koarashi, J., (2016) Modeling dynamics of ^{137}Cs in forest surface
1318 environments: application to a contaminated forest site near Fukushima and assessment of potential
1319 impacts of soil organic matter interactions. *Sci. Total Environ.*, 551–552: 590–604

- 1320 Pumpanen J., Ohashi M., Endo I., Hari P., Beack J., Kulmala M., Ohte N. (2016) ^{137}Cs
1321 distributions in soil and trees in forest ecosystems after the radioactive fallout - Comparison study
1322 between southern Finland and Fukushima, Japan. *Journal of Environmental Radioactivity*, 161: 73-81
- 1323 Rantavaara, A., Vetikko, V., Raitio, H., Aro, L., (2012) Seasonal variation of the ^{137}Cs level
1324 and its relationship with potassium and carbon levels in conifer needles. *Sc. Tot. Environ.* 441, 194-
1325 208
- 1326 Rühm W, Kammerer L, Hiersche L, Wirth E, (1996) Migration of ^{137}Cs and ^{134}Cs in different
1327 forest soil layers. *J Environ Radioact*, 33:63–75
- 1328 Saito, T., Makino, H., Tanaka, S., (2014) Geochemical and grain-size distribution of radioactive
1329 and stable cesium in Fukushima soils: implications for their long-term behavior. *J. Environ. Radioact.*,
1330 138: 11–18.
- 1331 Sanada Y., Sugita T., Nishizawa Y., Kondo A. and Torii T., (2014a) The aerial radiation
1332 monitoring in Japan after the Fukushima Daiichi nuclear power plant accident. *Progress in Nuclear*
1333 *Science and Technology*, 4: 76-80.
- 1334 Sanada Y. and Torii T., (2014b) Aerial radiation monitoring around the Fukushima Dai-ichi
1335 nuclear power plant using an unmanned helicopter. *Journal of Environmental Radioactivity*, 139:294-
1336 9.
- 1337 Schell, W.R., I. Linkov, C. Myttenaere and B. Morel. (1996) A dynamic model for evaluating
1338 radionuclide distribution in forests from nuclear accidents. *Health Phys.*, 70: 318-335
- 1339 Schimmack W, Bunzl K, (1992) Migration of radiocesium in two forest soils as obtained from
1340 field and column investigations. *Sci Total Environ*, 116:93–107
- 1341 Schimmack W., Forster H., Bunzl K., Kreutzer K. (1993) Deposition of radiocesium to the soil
1342 by stemflow, throughfall and leaf-fall from beech trees. *Radiat Environ Biophys.*, 32:137-150

- 1343 Shaw, G., Avila, R., Fesenko, S., Dvornik, A., Zhuchenko T., (2003) Modelling the behaviour
1344 of radioCesium in forest ecosystems. MODELLING RADIOACTIVITY IN THE ENVIRONMENT.
1345 E. Marian Scott (Editor) © 2003 Elsevier Science Ltd. All rights reserved.
- 1346 Shaw, G., Venter, A., Avila, R., Bergman, R., Bulgakov, A., Calmon, P., Fesenko, S., Frissel,
1347 M., Goor, F., Konoplev, A., Linkov, I., Mamikhin, S., Moberg, L., Orlov, A., Rantavaara, A.,
1348 Spridonov, S., Thiry, Y., (2005) Radionuclide migration in forest ecosystems. Results of a model
1349 validation study. *Journal of environmental radioactivity*, 84(2): 285-296.
- 1350 Shinomiya Y., Tamai K., Kobayashi M., Ohnuki Y., Shimizu T., Iida S., Nobuhiro T., Sawano
1351 S., Y. & Hiruta T. (2014) Radioactive cesium discharge in stream water from a small watershed in
1352 forested headwaters during a typhoon flood event. *Soil Science and Plant Nutrition*, 60 : 765–771.
- 1353 Shoko I., Hideki T., Tatsuhiko N. & Seiji H. (2017) Effect of mass of organic layers on variation
1354 in ¹³⁷Cs distribution in soil in different forest types after the Fukushima nuclear accident. *Journal of*
1355 *Forest Research*. DOI: 10.1080/13416979.2017.1418162
- 1356 Shutou K. & Nakane K. (2004) Change in soil carbon cycling for stand development of
1357 japanese cedar (*Cryptomeria japonica*) plantations following clear-cutting. *Ecological Research*,
1358 19(2):233–244.
- 1359 Sombré, L., Vanhouche, M., Ronneau, C., Lambotte, J.M., Myttenaere, C., (1994) Long-term
1360 radiocesium behaviour in spruce and oak Forests. *Sc. Tot. Environ.*, 157: 59-71
- 1361 Steiner M, Linkov I, Yoshida S. (2002) The role of fungi in the transfer and cycling of
1362 radionuclides in forest ecosystems. *J Environ Radioact*, 58:217–241
- 1363 Strebl F., Gerzabek M.H., Bossew P., Kienzl K., (1999) Distribution of radiocesium in an
1364 Austrian forest stand. *Sci Total Environ*, 226:75–83
- 1365 Sun X., Onda Y., Otsuki K., Kato H., Gomi T., Liu X. (2017) Change in evapotranspiration
1366 partitioning after thinning in a Japanese cypress plantation. *Trees*, 31:1411–1421

1367 Tagami, K., Uchida, S., Ishii, N., Kagiya, S., (2012) Translocation of radiocesium from stems
1368 and leaves of plants and the effect on Radiocesium activities in newly expanded plant tissues. J.
1369 Environ. Radioact., 111:65-69.

1370 Takada T., Yamada T., Takahara T., Okuda T., (2016) Spatial variation in the ¹³⁷Cs inventory
1371 in soils in a mixed deciduous forest in Fukushima, Japan. Journal of Environmental Radioactivity,
1372 161:35-41

1373 Takahashi J., Tamura K., Suda T., Matsumura R., Onda Y. (2015) Vertical distribution and
1374 temporal changes of ¹³⁷Cs in soil profiles under various land uses after the Fukushima Dai-ichi
1375 Nuclear Power Plant accident. Journal of Environmental Radioactivity, 139: 351-361.

1376 Takahashi, J., Onda, Y., Hihara, D., Tamura, K., (2018) Six-year monitoring of the vertical
1377 distribution of radiocesium in three forest soils after the Fukushima Dai-ichi Nuclear Power Plant
1378 accident. J. Environ. Radioact., 192:172–180.

1379 Tanaka K., Iwatani H., Sakaguchi A., Takahashi Y., Onda Y. (2013) Local distribution of
1380 radioactivity in tree leaves contaminated by fallout of the radionuclides emitted from the Fukushima
1381 Daiichi Nuclear Power Plant. J Radioanal Nucl Chem, 295:2007–2014

1382 Teramage M.T., Onda Y., Kato H., Gomi T. (2014a) The role of litterfall in transferring
1383 Fukushima-derived radiocesium to a coniferous forest floor. Science of the Total Environment, 490:
1384 435-439.

1385 Teramage, M.T., Onda, Y., Patin, J., Kato, H., Gomi, T., Nam, S., (2014b) Vertical distribution
1386 of radiocesium in coniferous forest soil after the Fukushima nuclear power plant accident. J. Environ.
1387 Radioact., 137: 37–45.

1388 Teramage, M.T., Onda, Y., Kato, H., (2016) Small scale temporal distribution in undisturbed
1389 coniferous forest soil: Radiocesium depth distribution profiles. J. Environ. Management, 170: 97-104.

1390 Teramage, M.T., Carasco, L., Coppin F. (2019a) Impact of drying and wetting cycles on ¹³⁷Cs
1391 ageing in forest soils contaminated with different input forms. J. Environ. Radioact., 203: 93–97.

- 1392 Teramage, M.T., Carasco, L., Orjollet, D., Coppin F. (2019b) The impact of radiocesium input
1393 forms on its extractability in Fukushima forest soils. *J. Hazardous Materials*, 349: 205–214.
- 1394 Thiry Y, Colle C, Yoschenko V, Levchuk S, Van Hees M, Hurtevent P, Kashparov V, (2009)
1395 Impact of Scot pine (*Pinus sylvestris* L.) plantings on long term ¹³⁷Cs and ⁹⁰Sr recycling from a
1396 waste burial site in the Chernobyl Red Forest. *J Environ Radioact*, 100:1062–1068
- 1397 Thiry Y., Albrecht A., Tanaka T., (2018) Development and assessment of a simple ecological
1398 model (TRIPS) for forests contaminated by radiocesium fallout. *Journal of Environmental*
1399 *Radioactivity*, 190–191 :149–159
- 1400 Thiry Y., Tanaka T., Dvornik A.A., Dvornik A.M., (2020) TRIPS 2.0: Toward more
1401 comprehensive modeling of radioCesium cycling in forest. *Journal of Environmental Radioactivity*
1402 214-215:106171
- 1403 Tikhomirov F.A. & Shcheglov A.I. (1991) The radioecological consequences of the Kyshtym
1404 and Chernobyl accidents for forest ecosystems (in Russian). *Proceedings of Seminar on Comparative*
1405 *Assessment of the Environment. Impact of Radionuclides Released during Three Major Nuclear*
1406 *Accidents: Kyshtym, Windscale, Chernobyl. Luxemburg, 1-5 october 1990, Rep. EUR 13574, 2, 867-*
1407 *887.*
- 1408 Tikhomirov F.A. & Shcheglov A.I., (1994) Main investigation results on the forest radioecology
1409 in the Kyshtym and Chernobyl accident zones. *The Science of the Total Environment*, 157, 45-57.
- 1410 Toriyama J., Kobayashi M., Hiruta T., Shichi K. (2018) Distribution of radiocesium in different
1411 density fractions of temperate forest soils in Fukushima. *Forest Ecology and Management*, 409: 260–
1412 266.
- 1413 Tsuruta K., Kosugi Y., Takanashi S. and Tani M. (2016) Inter-annual variations and factors
1414 controlling evapotranspiration in a temperate Japanese cypress forest. *Hydrol. Process.*, 30 : 5012–
1415 5026
- 1416 Wang W., Hanai Y., Takenaka C., Tomioka R., Iizuka K., Ozawa H., (2016) Cesium absorption
1417 through bark of Japanese cedar (*Cryptomeria japonica*). *Journal of Forest Research*, 21, 251-258.

- 1418 Yamashita T., Kasuya N., Nishimura S. & Takeda H. (2004) Comparison of two coniferous
1419 plantation in central japan with respect to forest productivity, growth phenology and soil nitrogen
1420 dynamics. *Forest Ecology and Management*, 200:215 – 226.
- 1421 Yoschenko, V., Takase, T., Konoplev, A., Nanba, K., Onda, Y., Kivva, S., Zheleznyak, M.,
1422 Sato, N., Keitoku, K., (2017) Radiocesium distribution and fluxes in the typical *Cryptomeria japonica*
1423 forest at the late stage after the accident at Fukushima Dai-ichi nuclear power plant. *J. Environ.*
1424 *Radioact.*, 166:45–55.
- 1425 Yoschenko, V., Takase, T., Hinton, T.G., Namba, K., Onda, Y., Konoplev, A., Goto, A.,
1426 Yokoyama, A., Keitoku, K., (2018) Radioactive and stable cesium isotope distributions and dynamics
1427 in Japanese cedar forests. *J. Environ. Radioact.*, 186: 34–44.
- 1428 Yoshida T. & Hijii N. (2006) Spatio-temporal distribution of aboveground litter in a
1429 *Cryptomeria japonica* plantation. *Journal of Forest Research* 11, 419–426
- 1430 Yoshihara T., Matsumura H., Hashida S., Nagaoka T. (2013) Radiocesium contaminations of
1431 20 wood species and the corresponding gamma-ray dose rates around the canopies at 5 months after
1432 the Fukushima nuclear power plant accident. *Journal of Environmental Radioactivity*, 115: 60-68.
- 1433 Yoshihara T., Matsumura H., Tsuzaki M., Wakamatsu T., Kobayashi T., Hashida S., Nagaoka
1434 T., Goto F. (2014) Changes in radiocesium contamination from Fukushima in foliar parts of 10
1435 common tree species in Japan between 2011 and 2013. *Journal of Environmental Radioactivity*, 138:
1436 220-226.
- 1437 Yoshihara T., Matsumura H., Hashida S., Nakaya K. (2016) Radiocesium contamination in
1438 living and dead foliar parts of Japanese cedar during 2011-2015. *Journal of Environmental*
1439 *Radioactivity*, 164: 291-299.
- 1440 Zhu Y.G. and Smolders E. (2000) Plant uptake of radiocaesium: a review of mechanisms,
1441 regulation and application, *J. Experimental Botany*, 51:1635–1645.
- 1442 Zimmermann, B., Zimmermann, A. , Lark, R. M., Elsenbeer, H. (2010) Sampling procedures
1443 for throughfall monitoring: A simulation study, *Water Resour. Res.*, 46: W01503

1

Table 1. List of the coniferous forest studies selected in the review.

Research group (ID)	Dominant species (number of sites)	Type of measurements available (*)	Reference
University of Tsukuba, Institute of Radioprotection and Nuclear Safety, France (KATO)	Cedar (3) Cypress (1)	TF, SF, LF Tree: S, C, M Soil: S, C	Kato et al. 2012, 2014, 2017, 2019; Hisadome et al. 2013; Teramage et al. 2014a,b, 2016, 2018, 2020; Loffredo et al. 2014, 2015; Takahashi et al. 2015, 2018; Coppin et al. 2016; Hurtevent et al. (in prep); Kurihara et al. 2018
Institute of Environmental Radioactivity, Fukushima (YOKO)	Cedar (2)	TF, SF, LF Tree: S, C, M Soil: S	Yoschenko et al. 2016, 2018
Forestry and Forest Products Research Institute, Tsukuba (KAJI)	Cedar (3) Cypress (2)	Tree: S, C, M Soil: S, C	Kaneko et al. 2013, Kuroda et al. 2013; Kajimoto et al. 2015; Komatsu et al. 2016, 2017; Imamura et al. 2017a,b; Ohashi et al. 2017; Manaka et al. 2019; Fujii et al. 2014, 2019
University of Tokyo, Chiba University (ENDO)	Cedar (1)	TF, SF, LF Tree: C	Endo et al. 2014, 2015; Murakami et al. 2014 ; Pumpanen et al. 2016
National Institute for Environmental Studies, Tsukuba (NISHI)	Cedar (2) Cypress (2)	TF, LF	Nishikiori et al. 2015, 2019
Forestry and Forest Products Research Institute, Tsukuba (ITOH)	Cedar (9) Cypress (1)	TF	Itoh et al. 2014, 2015
Japanese Atomic Energy Agency, Fukushima (NIIZA)	Cedar (1)	TF, SF, LF	Niizato et al. 2016
Forestry and Forest Products Research Institute, Chuo-ku (TORI)	Cypress/Cedar (1)	Soil: S, C	Shinomiya et al. 2014; Hiruta et al. 2016; Toriyama et al. 2018
National Institute for Environmental Studies, Tamuragunn (SHOKO)	Cedar (2) Cypress (1) Red pine (3)	Soil: S, C	Shoko et al. 2017
Japanese Atomic Energy Agency, Ibaraki (KOARA)	Cedar (2) Red pine (1)	Soil: S, C	Koarashi et al. 2012a,b, 2014, 2016a,b, 2019a,b; Matsunaga et al. 2013; Nakanishi et al. 2014; Ota et al. 2016; Muto et al. 2019
Gakushuin university, Tokyo (OHNO)	Cedar (1)	Soil: S, C	Ohno et al. 2012
Kyoto University (KANG)	Cedar (3)	Soil: S, C	Kang et al. 2017

2 (*) TF: throughfall ($\text{Bq m}^{-2} \text{d}^{-1}$), SF: stemflow ($\text{Bq m}^{-2} \text{d}^{-1}$), LF: litterfall ($\text{Bq m}^{-2} \text{d}^{-1}$), S: activity inventory in
3 soil horizons or tree organs (Bq m^{-2}), C: activity concentration in soil layers or tree organs (Bq kg^{-1}), M: surface
4 biomass of tree vegetation (kg m^{-2})
5

6
7

Table 2. Best estimates of the transfer rates (in d⁻¹) involved in the forest compartmental model for varying values of the interception fraction.

Transfer process (transfer rate)	Interception fraction			
	$f=0.70$	$f=0.75$	$f=0.80$	$f=0.85$
Root uptake (λ^{up})	$3.9 \cdot 10^{-5}$ (0.32) (*)	$2.7 \cdot 10^{-5}$ (0.33)	$1.5 \cdot 10^{-5}$ (0.34)	$<1 \cdot 10^{-6}$ (0.38)
Incorporation (λ^{inc})	$5.2 \cdot 10^{-5}$ (0.615)	$5.4 \cdot 10^{-5}$ (0.615)	$5.7 \cdot 10^{-5}$ (0.62)	$6 \cdot 10^{-5}$ (0.635)
Migration from surface layer (λ_{SL})	$1.25 \cdot 10^{-3}$ [1.1 - 1.32]** (8.9)	$1.27 \cdot 10^{-3}$ [1.15 - 1.34] (8.8)	$1.31 \cdot 10^{-3}$ [1.21 - 1.35] (8.7)	$1.35 \cdot 10^{-3}$ [1.32 - 1.36] (8.6)
Migration from 0-5cm layer (λ_{SS})	$2.2 \cdot 10^{-4}$ [1.35 - 5.5] (11.5)	$2.4 \cdot 10^{-4}$ [1.36 - 5.7] (12.0)	$2.7 \cdot 10^{-4}$ [1.38 - 5.8] (13.0)	$3 \cdot 10^{-4}$ [1.4 - 6] (13.5)
Migration from 5-10cm layer (λ_{S10})	$\sim 1 \cdot 10^{-3}$ [0.8 - 1.5] (40)	$\sim 1.2 \cdot 10^{-3}$ [1.0 - 1.7] (40)	$\sim 1.4 \cdot 10^{-3}$ [1.3 - 1.8] (39)	$\sim 1.6 \cdot 10^{-3}$ [1.5 - 2] (39)

8
9
10

(*) Value of the RMSLE (n.d.). (**) This range corresponds to the best estimates calculated for inventory and concentration separately (when not consistent).

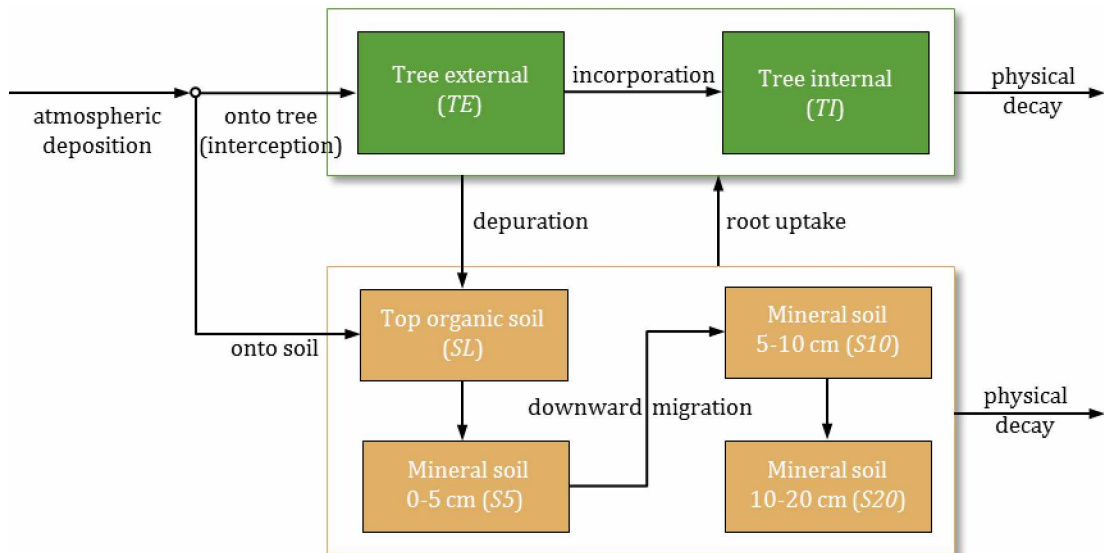


Figure 1. A simple compartmental model to evaluate the fate and transfer of radiocesium fallouts in an idealized forest stand, relying on 7 basic processes: atmospheric deposition, interception by the (above-ground) tree biomass, tree depuration, incorporation into internal tree organs, root uptake of bioavailable radiocesium, downward migration in soil and physical decay.

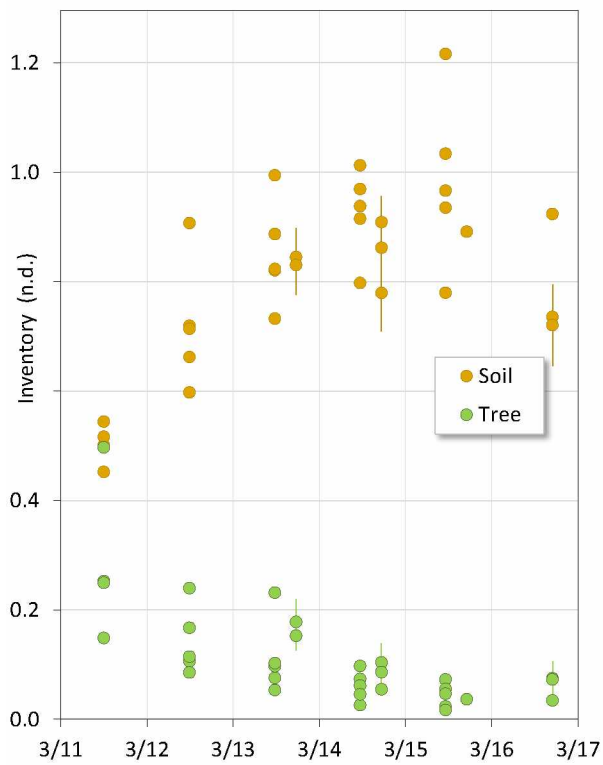


Figure 2. Time evolution of the site-specific activity inventories in soil and tree vegetation (8 sites, 2×33 data). Vertical bars represent GSDs.

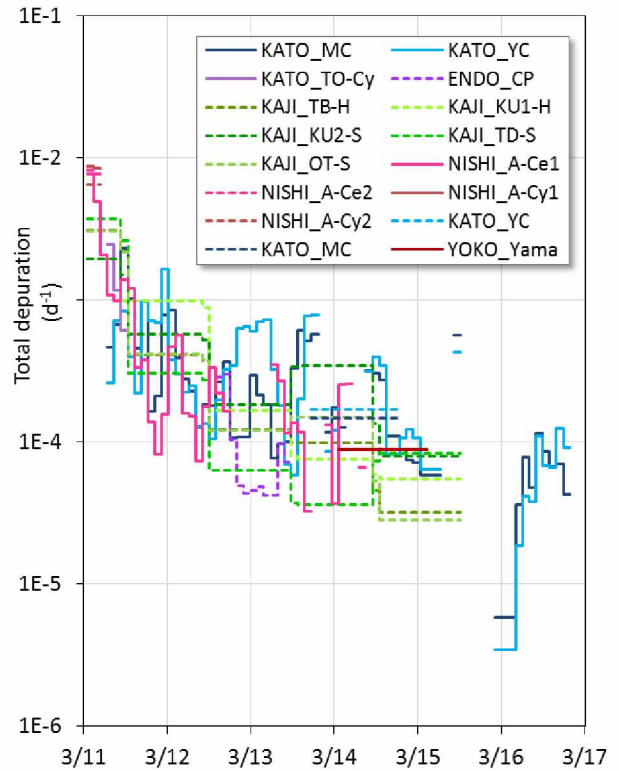


Figure 3. Time evolution of the site-specific activity depuration flux (14 sites), with the assumption that $f=0.85$ for KAJI sites.

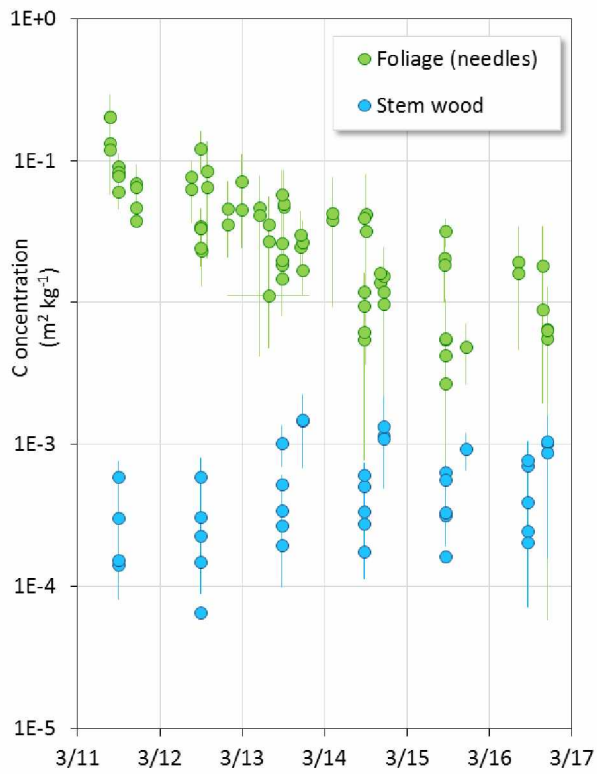


Figure 4. Time evolution of the site-specific activity concentrations in tree foliage and stem wood (9 sites, 70+35 data). Vertical bars represent GSDs.

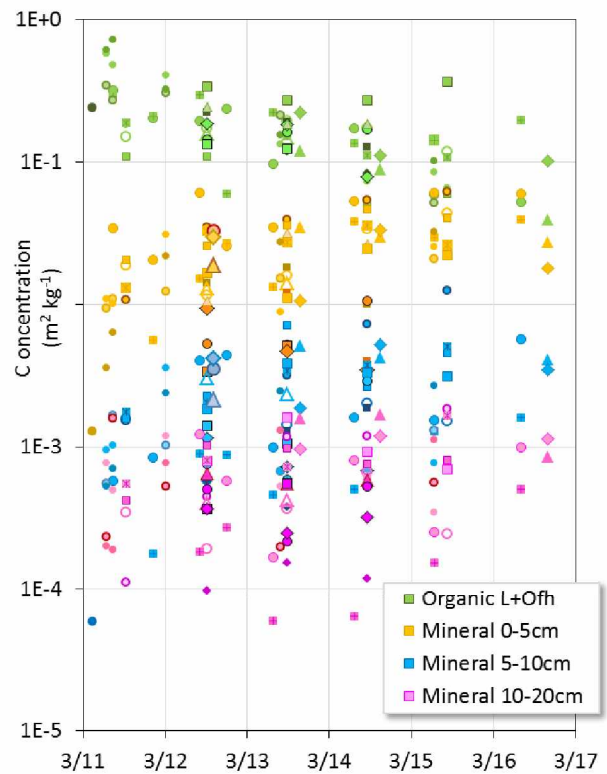


Figure 5. Time evolution of the site-specific activity concentrations in the organic and mineral soil layers (23 sites, about 4×80 data). GSDs are not displayed for graphical reasons.

15
16

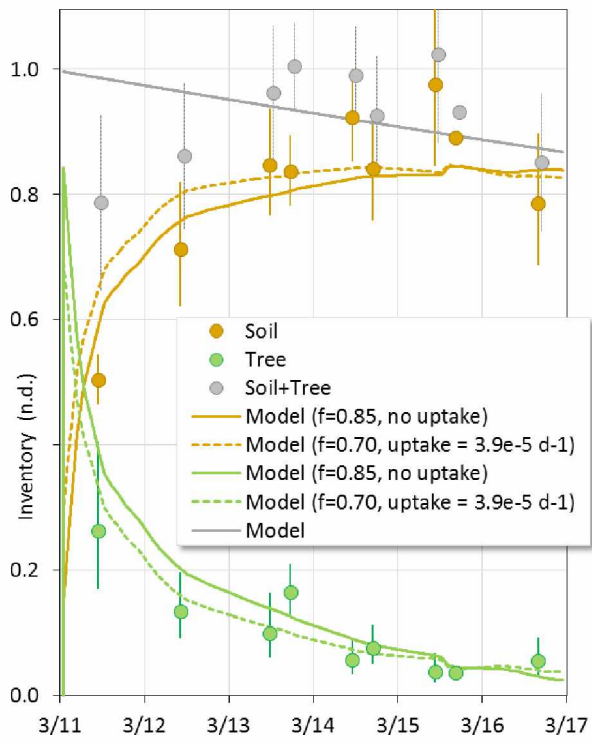


Figure 6. Time evolution of the mean activity inventories in soil and tree vegetation derived from data ($GM \pm GSD$) and predicted by the compartmental model with $f=0.70$ and 0.85 .

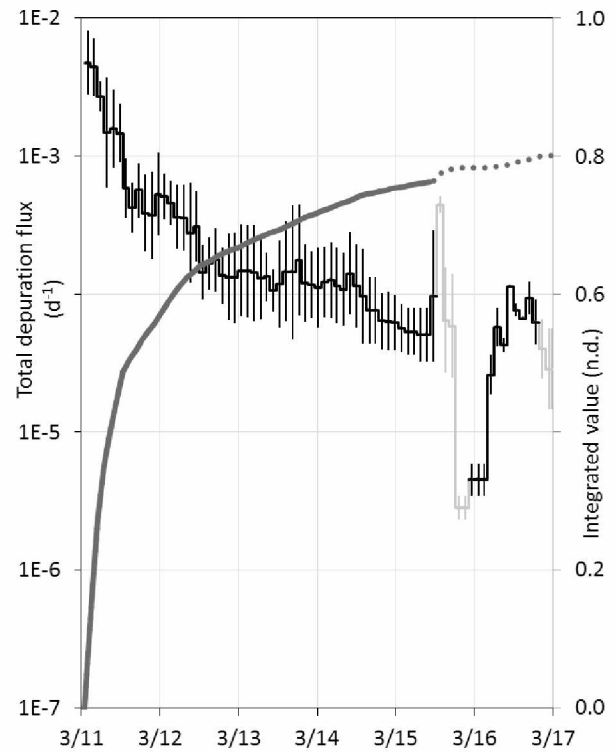
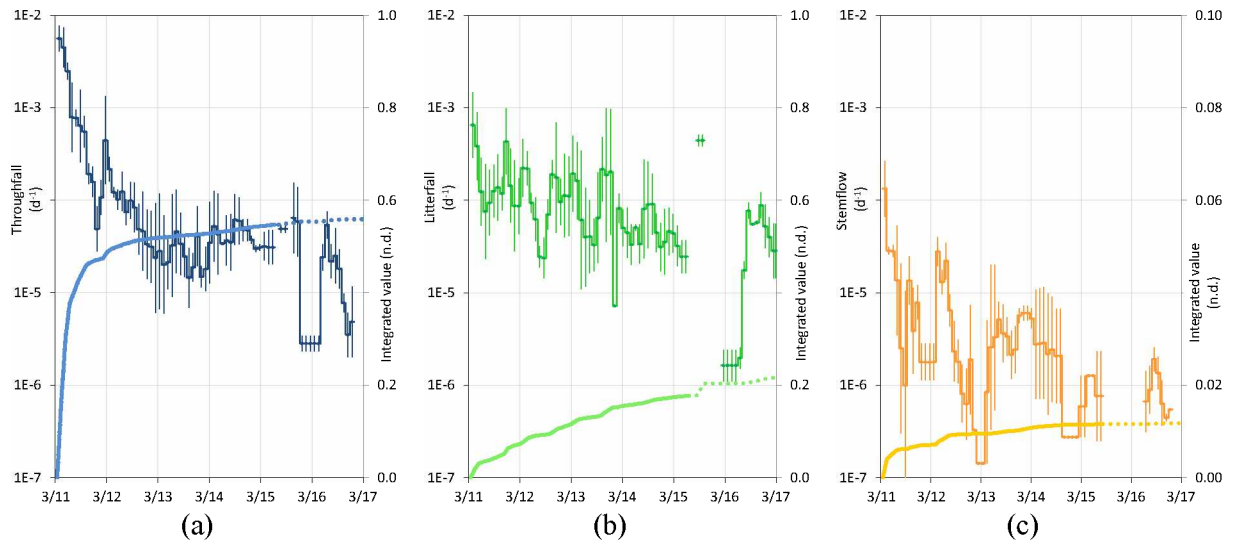


Figure 7. Time evolution of the mean total activity depuration flux derived from data ($GM \pm GSD$) and its cumulated value (GM), with the assumption that $f=0.85$ for KAJI sites. The grey portions indicate periods when throughfall or litterfall are missing.



19
20
21
22
23
24
25

Figure 8. Time evolution of the mean activity depuration fluxes derived from data ($GM \pm GSD$) and their cumulated values (GM): (a) throughfall, (b) litterfall and (c) stemflow. The dotted lines have been calculated by assuming that fluxes were nil in the absence of measurements.

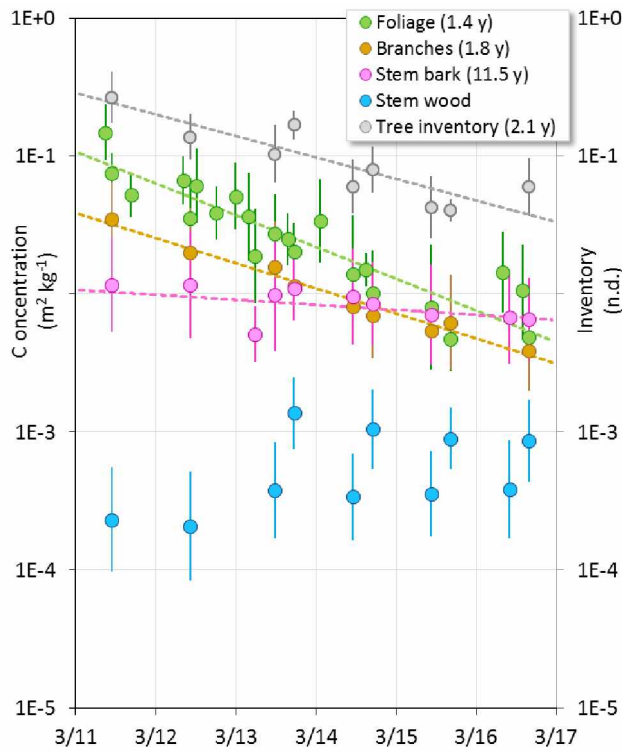


Figure 9. Time evolution of the mean activity concentrations in tree organs derived from data ($GM \pm GSD$), with indication of their effective half-lives.

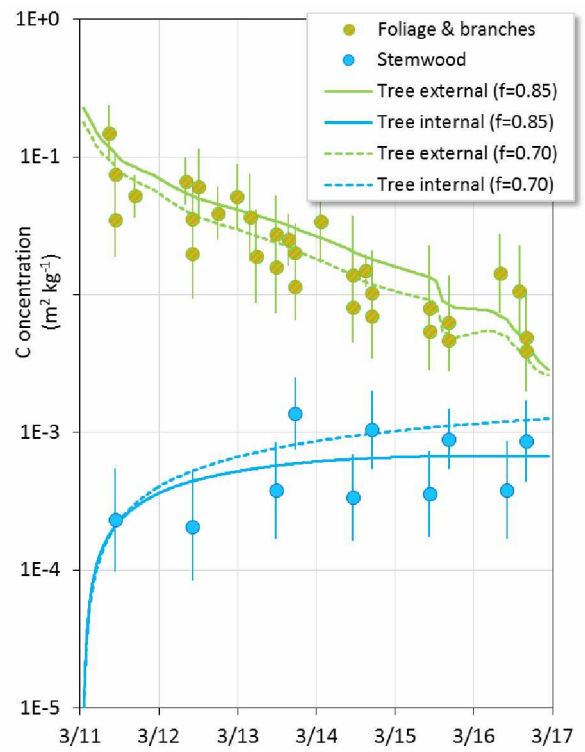


Figure 10. Time evolution of the activity concentrations in tree external and internal organs predicted by the compartmental model with $f=0.70$ and 0.85 (best estimates).

26
27
28

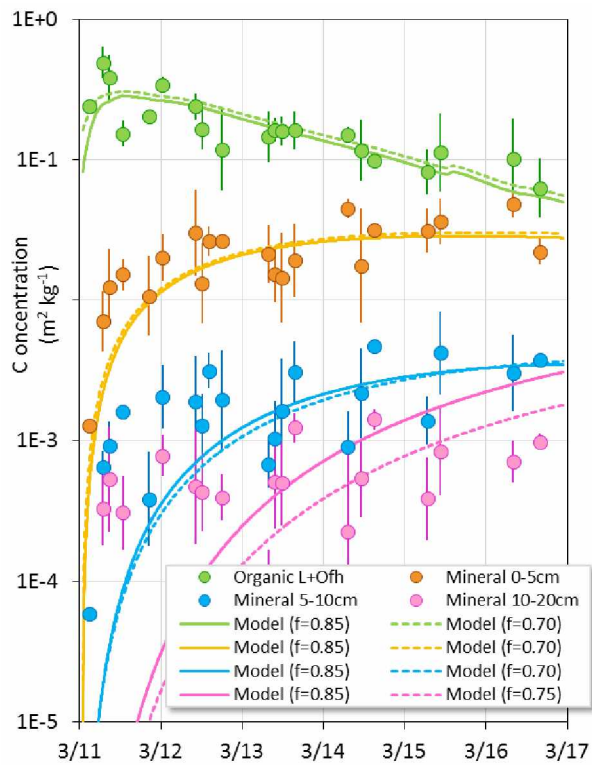


Figure 11. Time evolution of the mean activity concentrations in soil layers: derived from data (GM±GSD) and predicted by the compartmental model with $f=0.70$ and 0.85 (best estimates).

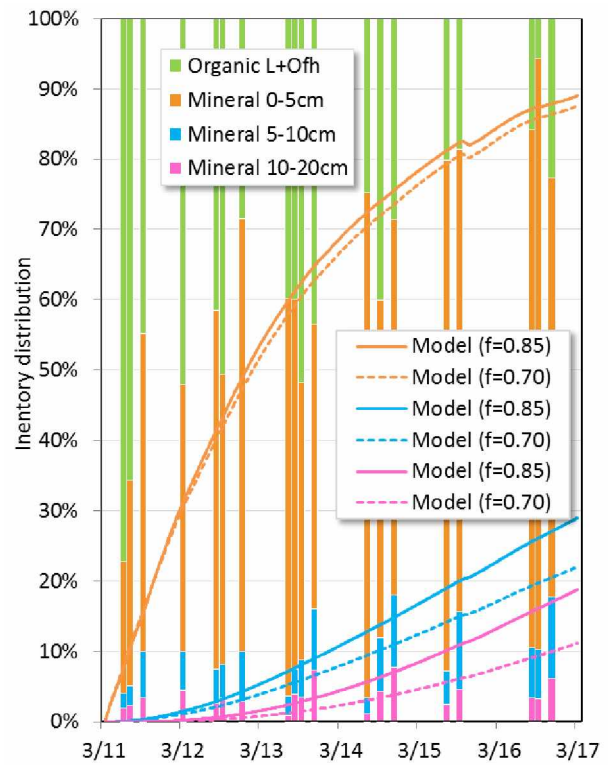


Figure 12. Time evolution of the mean activity partitioning between soil layers: derived from data (GM) and predicted by the compartmental model with $f=0.70$ and 0.85 (best estimates).

29

30

Supplementary material for on-line publication only

[Click here to download Supplementary material for on-line publication only: 2020_ForestCsDataReview_Manuscript_SI.docx](#)

Declaration of interests

The authors declare that they have no known competing financial interests or personal relationships that could have appeared to influence the work reported in this paper.

The authors declare the following financial interests/personal relationships which may be considered as potential competing interests: